A genome-wide screen identifies genes that suppress the accumulation of spontaneous mutations in young and aged yeast cells

Short Title: **A screen for mutation suppression genes in young and aged yeast cells**

Daniele Novarina[1], Georges E. Janssens[1], Koen Bokern[1], Tim Schut[1], Noor C. van Oerle[1], Hinke G. Kazemier[1], Liesbeth M. Veenhoff[1] and Michael Chang[1*]

[1]European Research Institute for the Biology of Ageing, University of Groningen, University Medical Center Groningen, Groningen, the Netherlands

[*]Corresponding author

E-mail: m.chang@umcg.nl (MC)

Abstract

To ensure proper transmission of genetic information, cells need to preserve and faithfully replicate their genome, and failure to do so leads to genome instability, a hallmark of both cancer and aging. Defects in genes involved in guarding genome stability cause several human progeroid syndromes, and an age-dependent accumulation of mutations has been observed in different organisms, from yeast to mammals. However, it is unclear if the spontaneous mutation rate changes during aging, and if specific pathways are important for genome maintenance in old cells. We developed a high-throughput replica-pinning approach to screen for genes important to suppress the accumulation of spontaneous mutations during yeast replicative aging. We found 13 known mutation suppression genes, and 31 genes that had no previous link to spontaneous mutagenesis, and all acted independently of age. Importantly, we identified *PEX19*, encoding an evolutionarily conserved peroxisome biogenesis factor, as an age-specific mutation suppression gene. While wild-type and *pex19Δ* young cells have similar spontaneous mutation rates, aged cells lacking *PEX19* display an elevated mutation rate. This finding suggests that functional peroxisomes are important to preserve genome integrity specifically in old cells, possibly due to their role in reactive oxygen species metabolism.

Author Summary

Spontaneous mutations arise as a consequence of improper repair of DNA damage caused by intracellular (i.e. toxic by-products of normal cellular metabolism or inaccurate DNA replication) or external (e.g. UV light or chemotherapy) sources. Elevated mutagenesis is implicated in tumorigenesis, and an age-dependent accumulation of mutations has been observed in many organisms. However, it is still unclear how and at which rate mutations accumulate during aging. It is also unknown if specific mechanisms exist that protect the genome of aged cells. We developed a high-throughput, genome-wide approach to identify genes that suppress the accumulation of mutations during yeast replicative aging. Yeast replicative aging refers to the decline in viability a single cell experiences with increasing number of mitotic divisions. We identified a number of new genes that counteract the accumulation of mutations independently of age. Moreover, we discovered that *PEX19*, a gene involved in the biogenesis of peroxisomes, is important to prevent the accumulation of mutations in aged cells. Since *PEX19* is conserved in humans, our work might help understand how human cells could better protect their genome from mutations during aging.

Introduction

Genomic instability, which refers to an increased rate of accumulation of mutations and other genomic alterations, is a hallmark, and a likely driving force, of tumorigenesis [1]. Genomic instability is also a hallmark of aging [2], as suggested by the age-related accumulation of mutations observed in yeast, flies, mice and humans [3], and highlighted by the fact that defects in DNA repair pathways result in human premature aging diseases [4]. However, whether genome instability has a causative role in aging is still controversial [3], and it is not known if aged cells rely more heavily on specific genome maintenance pathways.

Saccharomyces cerevisiae is a convenient model to study genomic instability and its relationship with aging, since genome maintenance pathways are evolutionary conserved [5,6] and a large number of genetic assays have been developed to study DNA repair and mutagenesis in budding yeast [6,7]. Furthermore, most aging-related cellular pathways, as well as lifespan-modulating environmental and genetic interventions, show a remarkable degree of conservation from yeast to mammals [8–10]. There are two main *S. cerevisiae* aging models: replicative aging refers to the decline in viability that a cell experiences with increasing number of mitotic divisions (a model for aging of mitotically active cells), while chronological aging refers to the decline in viability of a non-dividing cell as a function of time (a model for aging of post-mitotic cells) [11].

To identify genes and pathways involved in mutagenesis during yeast replicative aging, two main challenges need to be overcome. First, while *S. cerevisiae* is a leading model system for genetic and genomic studies and the availability of the yeast deletion collection makes this model organism particularly amenable for genome-wide genetic screens [12,13], cellular processes involving low-frequency events, such as point mutations, recombination events or gross chromosomal rearrangements, pose a specific technical challenge, since these events are barely detectable with standard genome-wide screening methods [14]. In a pioneering study,

Huang and colleagues performed a genome-wide screen for yeast genes that suppress the accumulation of spontaneous mutations in young cells by screening patches of large numbers of cells on solid media [15]. Patches of each strain of the deletion collection were replica-plated on media containing canavanine to detect canavanine-resistant (Can^R) colonies arising from spontaneous mutations at the *CAN1* locus. A similar approach was subsequently used in other screens for genes controlling genome integrity [5,16–18]. This strategy has proven to be effective but is extremely laborious. To overcome these limitations, we developed a screening strategy to detect low-frequency events, based on high-throughput replica pinning of high-density arrays of yeast colonies.

The second challenge to identify genes involved in mutagenesis during yeast replicative aging is the isolation aged cells, since they constitute a tiny fraction of an exponentially growing cell population. To allow the study of a cohort of aging mother cells, Lindstrom and Gottschling developed the Mother Enrichment Program (MEP), an inducible genetic system that prevents the proliferation of daughter cells (Fig 1A) [19]. Upon activation by estradiol, the Cre recombinase, which is under the control of a daughter-specific promoter, enters the nucleus and disrupts two genes essential for cell cycle progression (namely *UBC9* and *CDC20*), resulting in an irreversible arrest of daughter cells in G2/M, while mother cells are unaffected. Thus, in the absence of estradiol, MEP cells grow exponentially and form normal colonies on an agar plate, while upon addition of estradiol, linear growth occurs and microcolonies are formed. Occasionally, due to spontaneous mutations, the MEP is inactivated and cells become insensitive to estradiol: these cells are called “escapers” [19]. Escaper cells grow exponentially and form normal sized colonies even in the presence of estradiol.

We combined the MEP system with a high-throughput replica-pinning strategy to perform a genome-wide screen aimed at identifying genes important to suppress the accumulation of spontaneous mutations in replicatively aging yeast cells, using escaper

95 formation as a readout for spontaneous mutagenesis events. With our approach, we identified
96 several new mutation suppression genes that act independently of age. We also found that
97 *PEX19*, involved in peroxisome biogenesis, is an age-specific mutation suppression gene:
98 while wild-type and *pex19Δ* young cells have similar spontaneous mutation rates, the absence
99 of *PEX19* causes an elevated mutation rate specifically in old cells. We suggest that functional
100 peroxisomes protect the genome of aged cells from spontaneous mutagenesis.

Results

A high-throughput screen to identify genes important for suppressing spontaneous mutations during yeast replicative aging

We developed a high-throughput replica-pinning strategy that enables detection of low-frequency events and used it to perform a genome-wide screen for genes important for suppressing spontaneous mutations during yeast replicative aging (Fig 1). We introduced the MEP system into the yeast knockout (YKO) collection via Synthetic Genetic Array (SGA) technology [20]. The resulting MEP-YKO collection was pinned multiple times in parallel on estradiol-containing plates (18 replicates per knockout strain) to activate the MEP, and grown for one week (Fig 1C). An example of our experimental setting is shown in Fig 1B. If at any time during aging a MEP-inactivating mutation occurs, an escaper colony is formed. Each plate was then re-pinned on estradiol and grown for two days to detect escapers (escaper test). At this point, all MEP-proficient mother cells that have exhausted their replicative potential are not able to give rise to a colony; conversely, if escaper cells are present, a fully grown colony can be observed (Fig 1B and C). Our high-throughput replica-pinning method allows the semi-quantitative estimation of spontaneous mutation rates on the basis of escaper formation (Fig 1C). Since every plate of the MEP-YKO collection was pinned multiple times in parallel on estradiol, it is possible to calculate the frequency of escaper formation for each deletion mutant strain in the collection: an increased escaper frequency compared to wild-type control strains is an indication of a high spontaneous mutation rate (Fig 1D).

To validate our assumption that the escaper frequency of each strain is a proxy for the spontaneous mutation rate, we could make use of the fact that 72 strains from the YKO collection were derived from a parental strain carrying an additional mutation in the mismatch repair gene *MSH3* and are therefore expected to show increased spontaneous mutation rates, independently of the identity of the knockout gene [21]. In addition, 340 empty positions

126 randomly dispersed over the 14 plates of the MEP-YKO library were manually filled in with a
127 wild-type MEP control. In Fig 1D, an overview of the escaper frequencies of the whole MEP-
128 YKO collection is shown. Most of the strains have an escaper frequency between 10% and
129 40% (median: 27.8%). The wild-type control strains show a similar behavior (median: 22.2%),
130 but with the important difference that the wild-type escaper frequency never exceeds 72.2%.
131 In contrast, the escaper frequency of most of the *msh3* strains falls between 50% and 80%
132 (median: 55.6%), validating the rationale of our screening method.

133 We then used Cutoff Linked to Interaction Knowledge (CLIK) analysis [22] to
134 determine the cutoff for validation in an unbiased manner. The CLIK algorithm identified an
135 enrichment of highly interacting genes at the top of our list (ranked according to escaper
136 frequency), confirming the overall high quality of our screen (Fig 1E). The cutoff suggested
137 by CLIK corresponds to an escaper frequency of 75%, which, not surprisingly, is slightly
138 higher than the maximum escaper frequency observed in the wild-type controls (72.2%). To
139 further explore the overall quality of the screen, we set the cutoff at 75% escaper frequency
140 and performed phenotypic enrichment analysis using ScreenTroll, which examines the
141 similarity between genome-scale screens [23]. Predictably, the first overlap with our gene list
142 is the mutator screen performed by Huang and colleagues [15]. Furthermore, most of the top
143 overlapping screens are related to genome instability and DNA damage sensitivity (S1 Table).
144 Based on the threshold determined by CLIK, we proceeded to direct validation of all hits with
145 an escaper frequency higher than 75%.

146

147 **Identification of new genes that suppress the accumulation of mutations independently**
148 **of replicative age**

149 We first discarded as false positive all hits where the escaper-causing mutation(s) had occurred
150 before the beginning of the aging experiment (i.e. during the generation of the MEP-YKO

library and before the subsequent high-throughput replica-pinning step) as in these cases, an escaper frequency of 100% is not an indication of an extremely high mutation rate. By spotting serial dilutions of strains from the MEP-YKO library on estradiol-containing plates (S1 Fig), we found that 25/115 hits had escaped before the actual screen started (S1 File). We then set out to validate the remaining 90 putative mutator strains.

Spontaneous mutations can occur at any moment of the replicative lifespan and our experimental design does not allow us to discriminate if a high escaper frequency is an indication of an increased mutation rate already in young cells, or of an elevated age-dependent accumulation of mutations. To distinguish between these two possibilities, we performed fluctuation tests to measure the forward mutation rate at the endogenous *CAN1* locus, where any type of mutation that inactivates the *CAN1* gene confers canavanine resistance [24,25]. Since fluctuation tests are performed with logarithmically growing cultures, they measure the spontaneous mutation rate in an age-independent fashion (i.e. in young cells). Twelve of our hits had been previously validated [15], and therefore were not re-tested. Several genes identified in the aforementioned study (namely *CSM2*, *SHU1*, *TSA1* and *SKN7*) fell just below our 75% escaper frequency cutoff (S1 File). Importantly, we validated 13 new mutator mutants. Our screening strategy thus enabled us to identify new genes important for the suppression of spontaneous mutations independently of replicative age. The 26 genes whose deletion results in an increased *CAN1* mutation rate of at least 1.8-fold compared to wild type are listed in Table 1. We named this group of genes “general mutation suppression genes” because the corresponding knockout strains, besides showing an elevated escaper frequency in our screening setup, also display an increased mutation rate when tested in young cells with a second assay for spontaneous mutagenesis at a different genetic locus. Of the general mutation suppression genes identified, 16/26 have one or more human orthologs. As expected, these

175 genes are significantly enriched for Gene Ontology categories related to DNA damage
176 response, DNA repair and recombination (Fig 2 and S2 File).

177 **Table 1. List of validated general mutation suppression genes.**

	Gene deleted	Can^R rate (x 10^{-7})	Function	Human ortholog(s)[a]
1	*RAD27*	167.1[#]	DNA replication and repair	*FEN1, GEN1*
2	*PMS1*	79.9[#]	mismatch repair	*PMS1, PMS2*
3	*MSH2*	64.9[#]	mismatch repair	*MSH2*
4	*MLH1*	53.0[#]	mismatch repair	*MLH1*
5	*MME1*	45.1[#]	magnesium ion export from mitochondrion	
6	*RAD54*	37.9[#]	recombinational repair	*ATRX, RAD54B, RAD54L, RAD54L2*
7	*RAD57*	37.2[#]	recombinational repair	*XRCC3*
8	*RAD55*	35.8[#]	recombinational repair	
9	*MPH1*	29.5[b]	error-free bypass of DNA lesions	*FANCM*
10	*MSH6*	27.7[#]	mismatch repair	*MSH6*
11	***YGL177W***	27.6	dubious open reading frame (ovlp *MPT5*)	
12	***CRS5***	23.6	copper-binding metallothionein	
13	***VMA6***	22.5	V-ATPase	*ATP6V0D1, ATP6V0D2*
14	***GRX7***	21.7	oxidative stress response	
15	*PSY3*	20.4[#]	error-free DNA lesion bypass	
16	*OGG1*	17.6[#]	DNA repair	*OGG1*
17	*SHU2*	17.4[#]	error-free DNA lesion bypass	
18	***NAT3***	17.0	NatB N-terminal acetyltransferase	*NAA20*
19	***APL1***	16.3	vesicle mediated transport	
20	***MET18***	8.1	Fe-S cluster assembly	*MMS19*
21	***YLR358C***	8.0	unknown (ovlp *RSC2*)	
22	***DSS4***	5.4	post-Golgi vesicle-mediated transport	
23	***RLF2***	5.2	chromatin assembly complex	*CHAF1A*
24	***SRP40***	5.0	preribosome assembly or transport	*NOLC1*
25	***NUP84***	4.9	nuclear pore complex	*NUP107*
26	***RAD10***	4.9	DNA repair	*ERCC1*
	Wild type	2.6		

178

179 Genes in **bold** were newly identified; genes in regular font were previously identified [15,26]
180 [#] values from Huang et al. [15]; all other values were determined as described in the Materials
181 and Methods and are statistically supported (Student's t-test)
182 [a] Human orthologs of yeast genes are taken from the "*S. cerevisiae* to human ortholog pairs"
183 tool from the Rothstein Lab Tool Suite
184 (http://www.rothsteinlab.com/tools/scerevisiae_hsapien_orthologs)
185 [b] An elevated mutation rate for this mutant has been previously reported [26]
186

We then determined whether the 64 strains that do not show an elevated mutation rate at the *CAN1* locus would display an increase in the mutation rate if measured by escaper formation in the MEP genetic background. To do so, we performed a slightly modified version of the fluctuation test, where selective (i.e. estradiol-containing) plates are incubated for seven days and colonies are counted after two and seven days. Escaper colonies appearing after two days of incubation originate from mutations occurring prior to plating (i.e. in young cells), while all colonies appearing between day 2 and day 7 originate from a mutation event that occurred during replicative aging (see Materials and Methods for details). This experimental setup mimics the conditions in which the initial screen was performed and allows us to simultaneously measure the escaper formation rates in young cells and the age-dependent escaper formation frequencies. With this assay we identified 18 genes whose deletion results in an increased escaper formation rate of at least 1.8-fold compared to the wild type, independently of replicative age (i.e. based on colonies counted at day 2). We named these genes "MEP-specific mutation suppression genes", since the spontaneous mutation rate measured at the *CAN1* locus in the corresponding knockout mutants is indistinguishable from the wild type (Table 2). About half (8/18) of these genes have one or more human orthologs. Intriguingly, MEP-specific mutation suppression genes are enriched for members of the THO/TREX complex, which is involved in co-transcriptional mRNA export from the nucleus. This process is important in the interplay between transcriptional elongation and R-loop formation in yeast and mammalian cells [27,28] (Fig 3 and S2 File).

Table 2. List of validated MEP-specific mutation suppression genes

	Gene deleted	Escaper rate (x 10^{-7})[a]	Function	Human ortholog(s)[b]
1	*XRN1*	84.1	exoribonuclease	*XRN1*
2	*COS10*	54.6	turnover of plasma membrane proteins	
3	*NIP100*	52.1	dynactin complex	*CEP350, CLIP1, CLIP2, CLIP3, CLIP4*
4	*RPP1A*	34.4	ribosomal protein	*RPLP1*

5	*FMP45*	29.7	mitochondrial membrane protein	
6	*RPL13B*	26.3	ribosomal protein	*RPL13*
7	*HOP2*	25.2	meiosis	
8	*SAC3*	17.1	mRNA export (TREX complex)	*MCM3AP, SAC3D1*
9	*HBT1*	14.2	polarized cell morphogenesis	
10	*NFT1*	12.2	putative ABC transporter	
11	*SNF2*	7.9	SWI/SNF chromatin remodeling complex	*SMARCA2, SMARCA4*
12	*MFT1*	7.6	mRNA export (THO complex)	
13	*GTO3*	7.6	glutathione transferase	
14	*THP1*	7.2	mRNA export (TREX complex)	
15	*SEM1*	6.1	mRNA export / proteasome regulation	*SHFM1*
16	*YPL205C*	6.0	dubious open reading frame	
17	*THP2*	5.9	mRNA export (THO/TREX complex)	
18	*UBA4*	5.6	thio-modification of tRNA	*MOCS3, UBA5*
	Wild type	2.9		

[a] All values shown are statistically supported (Student's *t*-test)

[b] Human orthologs of yeast genes are taken from the "*S. cerevisiae* to human ortholog pairs" tool from the Rothstein Lab Tool Suite (http://www.rothsteinlab.com/tools/scerevisiae_hsapien_orthologs)

PEX19 suppresses age-dependent accumulation of mutations

At the end of our validation pipeline, we were left with four gene knockout strains that display no significant increase in forward mutation rate at the *CAN1* locus and in escaper formation rate in young cells (colonies counted at day 2) but show a higher age-dependent escaper frequency compared to wild type (colonies counted at day 7) (S2 Table). We were particularly interested in these genes, since our observations might indicate an age-dependent mutator phenotype. To validate these putative age-specific mutator mutants with an independent and more accurate method, we mechanically isolated young and aged mother cells by biotinylation and magnetic sorting and measured mutation frequencies at the *CAN1* locus in both cell populations [29]. Based on the Can^R frequencies in young cells, the replicative age (assessed by bud scar counting), and the mutation rate in young cells (previously determined by fluctuation test), we could calculate the expected Can^R frequencies in aged cells under the assumption that the mutation rate remains constant during replicative aging (see Materials and

Methods for details). By comparing the observed and the expected frequencies, it becomes clear if the mutation rate of a given strain is constant or varies as cells age.

To establish a reference, we tested wild type cells. Strikingly, the observed mutation frequency in aged cells (replicative age ~17) was lower than expected (Fig 4B and S2 Fig), suggesting a decrease in the spontaneous mutation rate during replicative aging. We then measured mutation frequencies in young and old cells from the four putative age-specific mutator strains. After the first test, three of these strains did not show any increase in age-dependent mutation frequency compared to the wild type and were therefore discarded as false positives (S3 Fig and S2 Fig). Conversely, age-dependent mutation frequency in the absence of *PEX19* was higher than in the wild type. We therefore repeated the test and confirmed that *pex19*Δ aged cells (replicative age ~15.5) display much higher mutation frequencies than expected (Fig 4 and S2 Fig). This result suggests that *PEX19*, encoding an evolutionarily conserved factor required for peroxisome biogenesis [30], suppresses age-dependent accumulation of mutations. We observed a similar effect after the deletion of *PEX3*, which causes the same peroxisome biogenesis defect as observed in the absence of *PEX19*, namely lack of detectable peroxisomal structures [31]. Mutation frequency in aged *pex3*Δ cells (replicative age ~13) was much higher than expected (S4 Fig), supporting the notion that functional peroxisomes contribute to genome maintenance during yeast replicative aging.

Discussion

S. cerevisiae is an outstanding model in which to perform genetic screens. However, there has been a lack of genome-wide, high-throughput screening techniques to detect low-frequency events (such as point mutations, recombination events and gross chromosomal rearrangements). These technical limitations, in combination with the difficulty to isolate large populations of replicative old cells, have so far hindered the study of genome maintenance during replicative aging.

Potential applications of the high-throughput replica-pinning methodology

We developed a high-throughput replica-pinning approach to screen for cellular processes involving low-frequency events, thus filling a technological gap in the yeast screening field. We applied this strategy to screen for genes controlling the accumulation of spontaneous mutations during yeast replicative aging, using the Mother Enrichment Program both as a tool to induce replicative aging and as a reporter for spontaneous mutation events (Fig 1). Key technical adjustments (see Material and Methods) were: a) the use of 1536 format pads to pin the MEP-YKO collection in 384 format on estradiol, so that a smaller number of cells (~1.5 x 10^4) was deposited on the plate, to prevent nutrient limitation during replicative aging; b) the MEP-YKO collection amplification by parallel high-throughput replica-pinning to analyze 18 colonies per strain; c) the one-week incubation time, which allowed accumulation of spontaneous mutations throughout replicative lifespan. In this way, we were able to monitor enough cell divisions to detect low-frequency mutation events. Furthermore, the analysis of 18 independent colonies allowed the use of escaper frequency as a proxy for the spontaneous mutation rate. Bioinformatic analysis and experimental confirmation indicated the high quality of the screen, thus validating our methodology.

It is worth noting that, even independently of the MEP and the replicative aging perspective, a similar high-throughput replica-pinning approach can be used to screen for genes involved in other genome stability-related processes. For instance, we recently applied this strategy to study spontaneous homologous recombination events (manuscript in preparation). Similarly, our replica-pinning strategy could be adapted to screen for genes controlling genome integrity in the chronological lifespan model [32,33]. More generally, this technique can be used to study any process involving low-frequency events for which genetically selectable reporters exist or can be developed. Examples include transient (loss of) gene silencing [34], transcription errors [35] and read-through at premature termination codons [36].

New general mutation suppression genes identified

Our screening setup was designed to allow simultaneous identification of age-independent and age-specific mutator mutants. We identified 13 new genes that suppress the accumulation of spontaneous mutations at the *CAN1* locus independently of age (Table 1). Some of these general mutation suppression genes (*RAD10* and *NUP84*) have defined roles in genome integrity [37–39]. For some other well-characterized genes, their role in preventing accumulation of mutations can be inferred from their molecular function. For instance, *MET18* has a conserved role in iron-sulfur (Fe/S) cluster assembly and insertion in several proteins involved in DNA replication and repair [40–42]. *RLF2*/*CAC1* encodes the largest subunit of the Chromatin Assembly Factor-I (CAF-1) complex, for which a role in DNA replication and repair of UV-induced DNA damage has been described [43–47].

For another group of new mutation suppression genes (*VMA6*, *GRX7*, *CRS5*, *NAT3*), their role in preventing accumulation of mutations might be more indirect. *VMA6* encodes a subunit of the evolutionary conserved vacuolar H^+-ATPase (V-ATPase), responsible for vacuole acidification and cellular pH regulation [48,49]. Defects in yeast V-ATPase result in

294 vacuole alkalinization and increased cytoplasm acidification [50], mitochondrial
295 depolarization and fragmentation [51,52], altered iron homeostasis [53] and chronic
296 endogenous oxidative stress [54]. This phenotype could potentially explain the elevated
297 spontaneous mutation rate of a *vma6*Δ mutant, due to compromised functioning of Fe/S cluster-
298 containing DNA replication and repair proteins as a consequence of mitochondrial
299 depolarization [42,55], and/or to DNA damage caused by increased endogenous oxidative
300 stress [56]. It would be interesting to test if disruption of other V-ATPase subunits causes the
301 same mutator phenotype.

302 The *CRS5* gene product is a copper- and zinc- binding metallothionein [57,58]. The
303 role of Crs5 in preventing spontaneous mutations is likely linked to its protective role against
304 endogenous oxidative stress, since scavenging of reactive oxygen species is a general function
305 of metallothioneins [59]. Crs5 might also directly protect DNA from copper-induced cleavage
306 [60]. The reported physical interaction between Crs5 and the peroxiredoxins Tsa1 and Tsa2,
307 responsible for preventing DNA damage and genome instability due to hydrogen peroxide and
308 organic peroxides generated during normal cell metabolism, further supports a role for Crs5 in
309 protecting the genome from oxidative damage [61,62].

310 Of particular interest is the mutation suppression genes *NAT3*, encoding the catalytic
311 subunit of the conserved NatB N-terminal acetyltransferase. *NAT3* was identified in a screen
312 for radiation sensitive mutants, and thereafter named *RAD56* [63,64]. Importantly, its human
313 homologue hNAT3 has been implicated in carcinogenesis [65,66]. Non-degradative protein N-
314 acetylation occurs co-translationally and can modulate protein folding, protein localization and
315 protein-protein interactions [67]. It is likely that Nat3 prevents the accumulation of
316 spontaneous mutations by ensuring the proper functioning of one (or more) of its targets.
317 Interestingly, among the identified substrates of yeast NatB, several are involved in DNA
318 metabolism, such as Pol31, Rnr4, Sml1, Nup84 [68–70]. Furthermore, many other factors

319 involved in DNA processing and repair contain the peptide sequence recognized by NatB and
320 are thus potential targets of Nat3 [71]. Further work will be needed to identify the relevant
321 target(s) for preventing accumulation of spontaneous mutations.

322 *GRX7* encodes a largely uncharacterized glutaredoxin localized in the cis-Golgi
323 [72,73]. How the disulfide bond-reducing activity of Grx7 in the Golgi affects spontaneous
324 mutation rate in unclear, even though functional links between the Golgi apparatus and genome
325 maintenance mechanisms have been suggested [74,75]. The *DSS4* gene product functions in
326 the post-Golgi secretory pathway, while *APL1* is involved in clathrin-mediated vesicle
327 transport. The elevated spontaneous mutation rate of *dss4*Δ and *apl1*Δ strains may indicate a
328 thus far unanticipated connection between genome stability and vesicle transport in the
329 secretory pathway. The remaining genes (*YGL177W*, *YLR358C*, and *SRP40*) are poorly
330 characterized and require further investigation.

331

332 **MEP-specific age-independent mutation suppression genes are enriched for genes related**
333 **to mRNA export**

334 We also identified 18 mutants that, despite an undetectable increase in the spontaneous
335 mutation rate at the *CAN1* locus, display an age-independent elevated escaper formation rate
336 (Table 2). This observation hints at a locus-specific increase in mutagenesis for this group of
337 mutator strains. The observation that MEP-specific mutation suppression genes are enriched
338 for genes involved in mRNA export from the nucleus (Fig 3 and S2 File) suggests the
339 involvement of R-loop-dependent genome instability [27,28]. R-loops form preferentially at
340 specific genomic locations and can cause genomic instability by exposing single-stranded
341 DNA tracts, triggering hyper-recombination and interfering with DNA replication [76].
342 Intriguingly, the exoribonuclease encoded by *XRN1*, our top MEP-specific mutation
343 suppression gene, has also been implicated in preventing R-loop-dependent genome instability

344 [77]. To confirm this hypothesis, one would need to examine the genomic features of the locus
345 or loci where mutations that give rise to escapers happen. It is assumed that escaper-originating
346 mutations occur at the *cre-EBD78* locus (since inactivating the Cre recombinase results in a
347 disruption of the MEP system), but the creators of the MEP already suggested that this is not
348 always the case, and other unknown endogenous loci might be involved in escaper formation
349 [19]. Indeed, our genetic analysis of a few escapers originating from a wild-type MEP strain
350 showed that the escaper phenotype does not always co-segregate with the *cre-EBD78* locus,
351 confirming that mutations occurring at other genomic loci can result in MEP inactivation and
352 escaper formation (S3 Table).
353
354 **A decrease in the spontaneous mutation rate in aged yeast cells**
355 To investigate age-dependent spontaneous mutagenesis, we first compared mutation
356 frequencies at the *CAN1* locus in young and old wt cells. Interestingly, *CAN1* mutation
357 frequencies in aged cells are lower than predicted, indicating that spontaneous mutation rate
358 decreases during replicative aging (Fig 4B). This might occur, for instance, if the efficiency of
359 a mutagenic DNA repair pathway, such as translesion synthesis [78], is reduced in old cells.
360 The same effect would be observed if an error-free repair pathway is upregulated during aging.
361 A similar decrease in the spontaneous mutation rate at the *CAN1* endogenous locus has been
362 previously reported, although the same study suggested that this effect could be locus-specific
363 [29].
364
365 **A role for peroxisomes in suppressing age-dependent accumulation of spontaneous**
366 **mutations**
367 To better understand age-dependent mutagenesis, our screen aimed at identifying genes—if
368 they exist—that prevent accumulation of spontaneous mutations specifically in old cells. We

showed that *PEX19* is one of these genes, since its deletion has no effect on mutagenesis in young cells, but causes an elevated accumulation of mutations in aged cells (Fig 4). To our knowledge, this is the first described case of an age-dependent mutation suppression gene, suggesting that some cellular pathways are particularly important in protecting the genome of old cells.

PEX19 is an evolutionary conserved gene which plays a key role in peroxisome biogenesis, and whose absence results in the lack of detectable peroxisomes [30,31]. Deletion of *PEX3*, another peroxisome biogenesis gene, causes the same age-specific mutator phenotype (S4 Fig), implying that functional peroxisomes are important to prevent age-dependent accumulation of mutations. The human orthologs of *PEX19* and *PEX3*, together with other peroxins, are mutated in Zellweger syndrome, a severe cerebro-hepato-renal peroxisome biogenesis disorder [79]. Peroxisomes are key organelles for the maintenance of the redox balance of the cell. On the one hand, they generate H_2O_2 as a consequence of fatty acid peroxidation; on the other hand, they contain a set of antioxidant enzymes and function therefore as reactive oxygen species (ROS) scavenging organelles [80]. Interestingly, loss of Pex19 in *D. melanogaster* causes ROS accumulation and mitochondrial damage, and a mouse model of Zellweger syndrome displays a similar phenotype [81,82]. Elevated endogenous ROS are known to induce genome instability [83,84].

How could peroxisomes potentially contribute to genome integrity maintenance in aged yeast cells? Several studies report an asymmetric ROS distribution between mother and daughter cell, resulting in ROS accumulation during replicative aging [85–87]. These elevated ROS levels are accompanied by an age-dependent hyperoxidation and inactivation of the peroxiredoxin Tsa1, a key antioxidant enzyme important for genome integrity and for suppression of mutations [15,62,83,84,88]. In this context, the role of peroxisomes in protecting the genome from endogenous oxidative stress might become crucial, due to the age-

dependent increase in ROS accumulation and the concomitant progressive failure of other redundant antioxidant systems that are active in young cells. Our observations suggest that deletion of *PEX19* has a synergistic effect with age, resulting in elevated spontaneous mutagenesis. Given the evolutionary conservation of this and many other peroxisome biogenesis factors, it would be interesting to test the contribution of peroxisomes in genome maintenance during mammalian cell aging and cancer development. Indeed, several studies have reported the absence of peroxisomes in cancer cells [89–91], suggesting a possible link between peroxisome biogenesis defects and tumorigenesis [92].

Materials and Methods

Yeast strains and growth conditions

Standard yeast media and growth conditions were used [93,94]. All yeast strains used in this study are derivatives of the BY4741 genetic background [95] and are listed in Table 3. DNY34 was obtained from Y7092 and UCC8773 by crossing and tetrad dissection. The *ice2*Δ*::kanMX* strain from the deletion collection (EUROSCARF) strain was crossed with strain UCC8774 by standard yeast genetics to create the strain DNY80. Strains DNY99, DNY101, DNY102 and DNY105 were constructed by standard PCR-mediated gene deletion in strain UCC8773.

Table 3. Yeast strains used in this study.

Strain name	Relevant genotype	Source
BY4741	*MAT***a** *his3*Δ*1 leu2*Δ*0 ura3*Δ*0 met15*Δ*0*	[95]
UCC8773	*MAT***a** *his3*Δ*1 leu2*Δ*0 ura3*Δ*0 lys2*Δ*0 ho*Δ*::Pscw11-cre-EBD78-natMX loxP-CDC20-intron-loxP-hphMX loxP-UBC9-loxP-LEU2*	[96]
UCC8774	*MAT*α *his3*Δ*1 leu2*Δ*0 ura3*Δ*0 trp1*Δ*63 ho*Δ*::Pscw11-cre-EBD78-natMX loxP-CDC20-intron-loxP-hphMX loxP-UBC9-loxP-LEU2*	[96]
Y7092	*MAT*α *his3*Δ*1 leu2*Δ*0 ura3*Δ*0 can1*Δ*::STE2pr-Sp_his5 lyp1*Δ *met15*Δ*0*	[97]
DNY34	*MAT*α *his3*Δ*1 leu2*Δ*0 ura3*Δ*0 can1*Δ*::STE2pr-Sp_his5 lyp1*Δ *met15*Δ*0 ho*Δ*::PSCW11-cre-EBD78-natMX loxP-UBC9-loxP-LEU2 loxP-CDC20-Intron-loxP-hphMX*	This study
DNY80	*MAT***a** *his3*Δ*1 leu2*Δ*0 ura3*Δ*0 lys2*Δ*0 met15*Δ*0 ho*Δ*::Pscw11-cre-EBD78-natMX loxP-CDC20-intron-loxP-hphMX loxP-UBC9-loxP-LEU2 ice2*Δ*::kanMX*	This study

DNY99	*MAT***a** *his3Δ1 leu2Δ0 ura3Δ0 lys2Δ0 met15Δ0 hoΔ::Pscw11-cre-EBD78-natMX loxP-CDC20-intron-loxP-hphMX loxP-UBC9-loxP-LEU2 pex19Δ::kanMX*	This study
DNY101	*MAT***a** *his3Δ1 leu2Δ0 ura3Δ0 lys2Δ0 met15Δ0 hoΔ::Pscw11-cre-EBD78-natMX loxP-CDC20-intron-loxP-hphMX loxP-UBC9-loxP-LEU2 rox3Δ::kanMX*	This study
DNY102	*MAT***a** *his3Δ1 leu2Δ0 ura3Δ0 lys2Δ0 met15Δ0 hoΔ::Pscw11-cre-EBD78-natMX loxP-CDC20-intron-loxP-hphMX loxP-UBC9-loxP-LEU2 atg23Δ::kanMX*	This study
DNY105	*MAT***a** *his3Δ1 leu2Δ0 ura3Δ0 lys2Δ0 met15Δ0 hoΔ::Pscw11-cre-EBD78-natMX loxP-CDC20-intron-loxP-hphMX loxP-UBC9-loxP-LEU2 pex3Δ::kanMX*	This study

412

413

414 **High-throughput replica-pinning screen**

415 High-throughput manipulation of high-density yeast arrays was performed with the RoToR-
416 HDA pinning robot (Singer Instruments). The Mother Enrichment Program (MEP) was
417 introduced into the *MAT***a** yeast deletion collection (EUROSCARF) through Synthetic Genetic
418 Array (SGA) methodology [97] using the DNY34 query strain. The procedure was performed
419 twice in parallel to generate two independent sets of MEP yeast deletion arrays in 384-colony
420 format. When a specific MEP mutant was missing in one of the arrays, it was manually pinned
421 over from the other set. Positions that were empty in both sets were filled with *his3Δ::kanMX*
422 control strains, unless they were kept empty for plate identification purposes. Colonies from
423 the two sets of MEP yeast deletion arrays were pinned onto YPD + G418 plates and incubated
424 for six hours at 30°C. Each plate of each set was then pinned onto nine YPD plates containing
425 1 μM estradiol (18 replicates in total). At this step, colonies were pinned in 384 format using
426 1536 format pads, so that a smaller number of cells was deposited to prevent nutrient limitation.

Plates were incubated for seven days at 30°C and then scanned with a flatbed scanner. Subsequently, each plate was pinned onto one YPD plate containing 1 μM estradiol and incubated for two days at 30°C before scanning ("escaper test"). Colony area measurement was performed using the ImageJ software package [98] and the ImageJ plugin ScreenMill Colony Measurement Engine [99], to assess colony circularity and size in pixels. The data was filtered to exclude artifacts by requiring a colony circularity score greater than 0.8. Colonies with a pixel area greater than 200 were considered escapers, and for each deletion strain, the ratio of escapers to total colonies in replica pinning experiments was used as the escaper frequency score.

Screen validation pipeline

Putative hits were initially analyzed by fluctuation test to measure the forward mutation rate at the endogenous *CAN1* locus. To do so, we used the strains from the YKO collection, because the strains from the MEP-YKO collection are *can1Δ*. At first, we performed one fluctuation test per strain. If the mutation rate was higher than 1.5-fold of the wild-type mutation rate, the test was repeated another two or three times.

For all the genes whose deletion does not cause an increase in the mutation rate at the *CAN1* locus, the corresponding knockout strains from the MEP-YKO collection were analyzed by fluctuation test to measure the escaper formation rate in young cells and the escaper formation frequency in replicatively aged cells. At first, we performed one fluctuation test per strain. If the escaper formation rate was higher than 1.5-fold of the wild-type escaper formation rate, the test was repeated another two or three times. In case no increase in escaper formation rate was detected but elevated age-dependent escaper formation frequencies were observed, the experiment was repeated another one or two times.

Strains that consistently displayed an elevated age-dependent escaper formation frequency were further validated by construction of a new knockout strain in a MEP *CAN1* background and by direct measurement of spontaneous mutation frequencies at the *CAN1* locus in young and aged cells. Each knockout strain was tested once. If the age-dependent mutation frequencies were not higher that the wild-type control, the strain was discarded as a false positive; if the age-dependent mutation frequencies were increased compared to the wild-type control, the experiment was repeated three times.

The identity of all validated strains from the YKO and MEP-YKO collections was confirmed by barcode sequencing as previously described [100].

Measurements of the spontaneous forward mutation rate at the *CAN1* locus

Single colonies were inoculated in 5 ml YPD and grown up to saturation (two days at 30°C). 100 µl were plated onto canavanine-containing SD medium (50 µg/ml) to identify forward mutations in *CAN1* and 50 µl of a 10^5-fold dilution was plated onto SD medium to count viable cells. Colonies were counted after two days of growth at 30°C and the spontaneous forward mutation rate at the *CAN1* locus was determined by fluctuation test from nine independent cultures using the method of the median [25,101]. Values represent the average of at least three independent experiments.

Measurements of spontaneous escaper formation rate and age-dependent escaper formation frequencies

Single colonies were inoculated in 5 ml YPD and grown up to saturation (two days at 30°C). 50 µl of a 50-fold dilution (or a higher dilution, when needed) were plated onto YPD plates containing 1 µM estradiol to identify escaper occurrence in young cells ("young plates"), 50 µl of a 500-fold dilution (or a higher dilution, when needed) were plated onto YPD plates

containing 1 µM estradiol to identify escapers occurrence in aging cells ("old plates"), and 50 µl of a 500000-fold dilution was plated onto YPD plates to count viable cell number. Colonies were counted after two days of growth at 30°C (for "young plates" and YPD plates) or after two and after seven days of growth at 30°C (for "old plates"). In "young plates", colonies that were smaller than the colonies growing on the corresponding YPD plate were not counted, because for those colonies the escaper-causing mutation occurred after plating. The spontaneous escaper formation rate in young cells was determined by fluctuation test from 7-10 independent cultures using the MSS-maximum-likelihood estimator method from the FALCOR fluctuation analysis calculator [102]. Values represent the average of at least three independent experiments. Age-dependent escaper formation frequencies was calculated by dividing the number of escaper colonies that appeared between day 2 and day 7 (on "old plates") by the number of viable cells plated (determined from the YPD plates).

Measurements of spontaneous mutation frequencies at the *CAN1* locus in young and aged cells

Isolation of young and aged cells was performed essentially as previously described [19,103]. 1.5 x 10^9 cells from a log-phase MEP culture were washed with cold phosphate buffered saline (PBS), resuspended in cold PBS containing 7 mg/ml Sulfo-NHS-LC-Biotin (Thermo Scientific) and incubated for 20 min at room temperature with gentle shaking. Biotinylated cells were then washed with PBS, resuspended in 250 ml of pre-warmed YPD medium and allowed to recover for 2 h at 30°C with shaking. Estradiol was added to a final concentration of 1 µM to induce the MEP (aging starts here). After 2 h of incubation at 30°C with shaking, 100 ml were harvested (young cells), while the rest of the culture (150 ml) was inoculated in a total volume of 1 L YPD containing 1 µM estradiol and 100 µg/ml ampicillin (to discourage bacterial contamination), and incubated at 30°C with shaking. Young cells were washed with

cold PBS, resuspended in 5 ml cold PBS and incubated with 100 µl streptavidin-coated BioMag beads (Qiagen) in a 5 ml LoBind tube (Eppendorf) at 4°C with gentle shaking for 30 min. Cells were gently pelleted at 4°C (3 min 1800 × g), resuspended in 7 ml cold YPD and transferred to a glass test tube (Lab Logistics Group). The tube was placed in a magnet ("The Big Easy" EasySep Magnet, Stemcell Technologies) for 5 min on ice. Cells were then washed three times by removing supernatant by pipetting, resuspending them in 7 ml cold YPD and incubating for 5 min on ice in the magnet. Finally, cells were resuspended in 5.2 ml PBS and transferred in a 5 ml LoBind tube (Eppendorf). Of the 5.2 ml of purified mother cells, 100 µl were stained for bud scars counting (see below); 100 µl were diluted 1000x and plated on SD medium to assess cell viability; the remaining 5 ml were pelleted and plated on canavanine-containing SD medium (50 µg/ml) to identify forward mutations in *CAN1*. After 20 h of MEP induction, the entire aged 1 L culture was harvested. The aged cells were processed similarly to the young cells, with slight modifications because of the higher number of cells due to the presence of daughter cells. For beading, the cells were split into 4 different 5 ml LoBind tubes, and 50 µl streptavidin coated BioMag beads were added to each tube. For magnetic sorting, two glass tubes were used and cells were washed four times.

For both young and aged samples, colonies were counted after 2 d of growth at 30°C and the spontaneous forward mutation frequencies at the *CAN1* locus were determined. Expected mutation frequencies in aged cells were calculated as previously described [29].

Bud scar detection and counting

Purified mother cells (see above) were stained with propidium iodide (PI) (Sigma) to identify viable cells and with Calcofluor White (Fluorescent Brightener 28, Sigma) to detect bud scars. 100 µl of purified mother cells in PBS (~5 x 10^5 cells) were stained with 2 µl of a 2 mM PI (Sigma) solution for 30 min at 30°C. Cells were then washed with ddH_2O, fixed in 500 µl of

3.7% formaldehyde for 30 min at room temperature, washed with PBS, resuspended in 100 µl PBS and stored at 4°C. Just before imaging, cells were stained with Calcofluor White for 5 min at room temperature, washed with PBS and resuspended in 5-10 µl PBS. Images were acquired using a DeltaVision Elite imaging system (Applied Precision (GE), Issaquah, WA, USA) composed of an inverted microscope (IX-71; Olympus) equipped with a Plan Apo 100X oil immersion objective with 1.4 NA, InsightSSITM Solid State Illumination, excitation and emission filters for DAPI and A594, ultimate focus and a CoolSNAP HQ2 camera (Photometrics, Tucson, AZ, USA). Stacks of 30 images with 0.2 µm spacing were taken at an exposure time of 5 ms at 10% intensity for DAPI (Calcofluor White staining) and 50 ms at 32% intensity for A594 (PI staining). Reference bright-field images were also taken. Fluorescent images were subjected to 3D deconvolution using SoftWoRx 5.5 software (Applied Precision). Processing of all images was performed using Fiji (ImageJ, National Institute of Health) [98]. Bud scars from at least 50 PI-negative cells (which were alive after magnetic sorting) were manually counted for each sample to determine the cells' replicative age.

Gene Ontology enrichment analysis and functional annotation

GO enrichment analysis was performed with DAVID 6.8 (https://david.ncifcrf.gov/home.jsp) using the Functional Annotation tool [104,105]. To reduce functional redundancy among GO terms, we used the REVIGO Web server (http://revigo.irb.hr/) with a cutoff value C = 0.5 [106].

Functional enrichment within the yeast global genetic similarity network was performed and visualized with TheCellMap.org (http://thecellmap.org/), using SAFE [107,108].

Acknowledgments

We thank Marlien Visser for helping with the fluctuation tests and Grant W. Brown for critically reading the manuscript.

552 # References

553 1. Hanahan D, Weinberg RA. Hallmarks of cancer: the next generation. Cell. 2011;144:
554 646–674. doi:10.1016/j.cell.2011.02.013

555 2. López-Otín C, Blasco MA, Partridge L, Serrano M, Kroemer G. The hallmarks of aging.
556 Cell. 2013;153: 1194–1217. doi:10.1016/j.cell.2013.05.039

557 3. Moskalev AA, Shaposhnikov M V., Plyusnina EN, Zhavoronkov A, Budovsky A, Yanai
558 H, et al. The role of DNA damage and repair in aging through the prism of Koch-like
559 criteria. Ageing Res Rev. 2013;12: 661–684. doi:10.1016/j.arr.2012.02.001

560 4. Carrero D, Soria-Valles C, López-Otín C. Hallmarks of progeroid syndromes: lessons
561 from mice and reprogrammed cells. Dis Model Mech. 2016;9: 719–735.
562 doi:10.1242/dmm.024711

563 5. Putnam CD, Srivatsan A, Nene R V, Martinez SL, Clotfelter SP, Fonseca F, et al. A
564 genetic network that suppresses genome rearrangements in *Saccharomyces cerevisiae*
565 and contains defects in cancers. Nat Commun. 2016;7: 11256.
566 doi:10.1038/ncomms11256

567 6. Putnam CD, Kolodner RD. Pathways and mechanisms that prevent genome instability
568 in *Saccharomyces cerevisiae*. Genetics. 2017;206: 1187–1225.
569 doi:10.1534/genetics.112.145805

570 7. Symington LS, Rothstein R, Lisby M. Mechanisms and regulation of mitotic
571 recombination in *Saccharomyces cerevisiae*. Genetics. 2014;198: 795–835.
572 doi:10.1534/genetics.114.166140

573 8. Pitt JN, Kaeberlein M. Why is aging conserved and what can we do about it? PLoS Biol.
574 2015;13: e1002131. doi:10.1371/journal.pbio.1002131

575 9. Fontana L, Partridge L, Longo VD. Extending healthy life span — from yeast to humans.
576 Science. 2010;328: 321–326. doi:10.1126/science.1172539

10. Janssens GE, Veenhoff LM. Evidence for the hallmarks of human aging in replicatively aging yeast. Microb Cell. 2016;3: 263–274. doi:10.15698/mic2016.07.510

11. Denoth Lippuner A, Julou T, Barral Y. Budding yeast as a model organism to study the effects of age. FEMS Microbiol Rev. 2014;38: 300–325. doi:10.1111/1574-6976.12060

12. Giaever G, Nislow C. The yeast deletion collection: a decade of functional genomics. Genetics. 2014;197: 451–465. doi:10.1534/genetics.114.161620

13. Botstein D, Fink GR. Yeast: an experimental organism for 21st Century biology. Genetics. 2011;189: 695–704. doi:10.1534/genetics.111.130765

14. Chang M, Parsons AB, Sheikh B, Boone C, Brown GW. Genomic approaches for identifying DNA damage response pathways in *S. cerevisiae*. Methods Enzymol. 2006;409: 213–235. doi:10.1016/S0076-6879(05)09013-0

15. Huang M-E, Rio A-G, Nicolas A, Kolodner RD. A genomewide screen in *Saccharomyces cerevisiae* for genes that suppress the accumulation of mutations. Proc Natl Acad Sci U S A. 2003;100: 11529–11534. doi:10.1073/pnas.2035018100

16. Smith S, Hwang J, Banerjee S, Majeed A, Gupta A, Myung K. Mutator genes for suppression of gross chromosomal rearrangements identified by a genome-wide screening in *Saccharomyces cerevisiae*. Proc Natl Acad Sci U S A. 2004;101: 9039–9044. doi:10.1073/pnas.0403093101

17. Zhang Y, Shishkin AA, Nishida Y, Marcinkowski-Desmond D, Saini N, Volkov K V, et al. Genome-wide screen identifies pathways that govern GAA/TTC repeat fragility and expansions in dividing and nondividing yeast cells. Mol Cell. 2012;48: 254–265. doi:10.1016/j.molcel.2012

18. Zhang Y, Saini N, Sheng Z, Lobachev KS. Genome-wide screen reveals replication pathway for quasi-palindrome fragility dependent on homologous recombination. PLoS Genet. 2013;9: e1003979. doi:10.1371/journal.pgen.1003979

602 19. Lindstrom DL, Gottschling DE. The mother enrichment program: a genetic system for
603 facile replicative life span analysis in *Saccharomyces cerevisiae*. Genetics. 2009;183:
604 413–422. doi:10.1534/genetics.109.106229
605 20. Tong AHY, Boone C. Synthetic genetic array analysis in *Saccharomyces cerevisiae*.
606 Methods Mol Biol. 2006;313: 171–192.
607 21. Lehner KR, Stone MM, Farber RA, Petes TD. Ninety-six haploid yeast strains with
608 individual disruptions of Open Reading Frames between *YOR097C* and *YOR192C*,
609 constructed for the *Saccharomyces* Genome Deletion Project, have an additional
610 mutation in the Mismatch Repair gene *MSH3*. Genetics. 2007;177: 1951–1953.
611 doi:10.1534/genetics.107.079368
612 22. Dittmar JC, Pierce S, Rothstein R, Reid RJD. Physical and genetic-interaction density
613 reveals functional organization and informs significance cutoffs in genome-wide
614 screens. Proc Natl Acad Sci U S A. 2013;110: 7389–7394.
615 doi:10.1073/pnas.1219582110
616 23. Thorpe PH, Dittmar JC, Rothstein R. ScreenTroll : a searchable database to compare
617 genome-wide yeast screens. Database (Oxford). 2012;2012: bas022.
618 doi:10.1093/database/bas022
619 24. Reenan RAG, Kolodner RD. Characterization of insertion mutations in the
620 *Saccharomyces cerevisiae MSH1* and *MSH2* genes: evidence for separate mitochondrial
621 and nuclear functions. Genetics. 1992;132: 975–985.
622 25. Foster PL. Methods for determining spontaneous mutation rates. Methods Enzymol.
623 2006;409: 195–213. doi:10.1016/S0076-6879(05)09012-9
624 26. Scheller J, Schürer A, Rudolph C, Hettwer S, Kramer W. *MPH1*, a yeast gene encoding
625 a DEAH protein, plays a role in protection of the genome from spontaneous and
626 chemically induced damage. Genetics. 2000;155: 1069–1081.

627 27. Huertas P, Aguilera A. Cotranscriptionally formed DNA:RNA hybrids mediate
628 transcription elongation impairment and transcription-associated recombination. Mol
629 Cell. 2003;12: 711–721. doi:10.1016/j.molcel.2003.08.010
630 28. Domínguez-Sánchez M, Barroso S, Gómez-González B, Luna R, Aguilera A. Genome
631 instability and transcription elongation impairment in human cells depleted of
632 THO/TREX. PLoS Genet. 2011;7: e1002386. doi:10.1371/journal.pgen.1002386
633 29. Patterson MN, Maxwell PH. Combining magnetic sorting of mother cells and
634 fluctuation tests to analyze genome instability during mitotic cell aging in
635 *Saccharomyces cerevisiae*. J Vis Exp. 2014;92: e51850. doi:10.3791/51850
636 30. Agrawal G, Subramani S. De novo peroxisome biogenesis: evolving concepts and
637 conundrums. Biochim Biophys Acta. 2016;1863: 892–901.
638 doi:10.1016/j.bbamcr.2015.09.014
639 31. Hettema EH, Girzalsky W, Van Den Berg M, Erdmann R, Distel B. *Saccharomyces*
640 *cerevisiae* Pex3p and Pex19p are required for proper localization and stability of
641 peroxisomal membrane proteins. EMBO J. 2000;19: 223–233.
642 doi:10.1093/emboj/19.2.223
643 32. Powers III RW, Kaeberlein M, Caldwell SD, Kennedy BK, Fields S. Extension of
644 chronological life span in yeast by decreased TOR pathway signaling. Genes Dev.
645 2006;20: 174–184. doi:10.1101/gad.1381406
646 33. Wei M, Madia F, Longo VD. Studying age-dependent genomic instability using the *S.*
647 *cerevisiae* chronological lifespan model. J Vis Exp. 2011;55: e3030. doi:10.3791/3030
648 34. Dodson AE, Rine J. Heritable capture of heterochromatin dynamics in *Saccharomyces*
649 *cerevisiae*. Elife. 2015;4: e05007. doi:10.7554/eLife.05007
650 35. Gout J, Li W, Fritsch C, Li A, Haroon S, Singh L, et al. The landscape of transcription
651 errors in eukaryotic cells. Sci Adv. 2017;3: e1701484. doi:10.1126/sciadv.1701484

652 36. Altamura E, Borgatti M, Finotti A, Gasparello J, Gambari R, Spinelli M, et al. Chemical-
653 induced read-through at premature termination codons determined by a rapid dual-
654 fluorescence system based on *S. cerevisiae*. PLoS One. 2016;11: e0154260.
655 doi:10.1371/journal.pone.0154260
656 37. Schiestl RH, Prakash S. *RAD10*, an excision repair gene of *Saccharomyces cerevisiae*,
657 is involved in the *RAD1* pathway of mitotic recombination. Mol Cell Biol. 1990;10:
658 2485–2491. doi:10.1128/MCB.10.6.2485
659 38. Bardwell AJ, Bardwell L, Tomkinson AE, Friedberg EC. Specific cleavage of model
660 recombination and repair intermediates by the yeast Rad1-Rad10 DNA endonuclease.
661 Science. 1994;265: 2082–2085. doi:10.1126/science.8091230
662 39. Freudenreich CH, Su XA. Relocalization of DNA lesions to the nuclear pore complex.
663 FEMS Yeast Res. 2016;16: fow095. doi:10.1093/femsyr/fow095
664 40. Stehling O, Vashisht AA, Mascarenhas J, Jonsson ZO, Sharma T, Netz DJA, et al.
665 MMS19 assembles iron-sulfur proteins required for DNA metabolism and genomic
666 integrity. Science. 2012;337: 195–199. doi:10.1126/science.1219723
667 41. Gari K, León Ortiz MA, Borel V, Flynn H, Skehel JM, Boulton SJ. MMS19 links
668 cytoplasmic iron-sulfur cluster assembly to DNA metabolism. Science. 2012;337: 243–
669 245. doi:10.1126/science.1219664
670 42. Zhang C. Essential functions of iron-requiring proteins in DNA replication, repair and
671 cell cycle control. Protein Cell. 2014;5: 750–760. doi:10.1007/s13238-014-0083-7
672 43. Kaufman PD, Kobayashi R, Stillman B. Ultraviolet radiation sensitivity and reduction
673 of telomeric silencing in *Saccharomyces cerevisiae* cells lacking chromatin assembly
674 factor-I. Genes Dev. 1997;11: 345–357. doi:10.1101/gad.11.3.345
675 44. Game JC, Kaufman PD. Role of *Saccharomyces cerevisiae* chromatin assembly factor-
676 I in repair of ultraviolet radiation damage in vivo. Genetics. 1999;151: 485–497.

677 45. Smith S, Stillman B. Stepwise assembly of chromatin during DNA replication in vitro.
678 EMBO J. 1991;10: 971–980. doi:10.1002/j.1460-2075.1991.tb08031.x
679 46. Zhang Z, Shibahara KI, Stillman B. PCNA connects DNA replication to epigenetic
680 inheritance in yeast. Nature. 2000;408: 221–225. doi:10.1038/35041601
681 47. Moggs JG, Grandi P, Quivy J-P, Jonsson ZO, Hubscher U, Becker PB, et al. A CAF-1-
682 PCNA-mediated chromatin assembly pathway triggered by sensing DNA damage. Mol
683 Cell Biol. 2000;20: 1206–1218. doi:10.1128/MCB.20.4.1206-1218.2000
684 48. Bauerle C, Ho MN, Lindorfer MA, Stevens TH. The *Saccharomyces cerevisiae VMA6*
685 gene encodes the 36-kDa subunit of the vacuolar H^+-ATPase membrane sector. J Biol
686 Chem. 1993;268: 12749–12757.
687 49. Kane PM. The where, when, and how of organelle acidification by the yeast vacuolar
688 H^+-ATPase. Microbiol Mol Biol Rev. 2006;70: 177–191. doi:10.1128/MMBR.70.1.177
689 50. Martínez-Muñoz GA, Kane P. Vacuolar and plasma membrane proton pumps
690 collaborate to achieve cytosolic pH homeostasis in yeast. J Biol Chem. 2008;283:
691 20309–20319. doi:10.1074/jbc.M710470200
692 51. Merz S, Westermann B. Genome-wide deletion mutant analysis reveals genes required
693 for respiratory growth, mitochondrial genome maintenance and mitochondrial protein
694 synthesis in *Saccharomyces cerevisiae*. Genome Biol. 2009;10: R95. doi:10.1186/gb-
695 2009-10-9-r95
696 52. Hughes AL, Gottschling DE. An early age increase in vacuolar pH limits mitochondrial
697 function and lifespan in yeast. Nature. 2012;492: 261–265. doi:10.1038/nature11654
698 53. Diab HI, Kane PM. Loss of vacuolar H^+-ATPase (V-ATPase) activity in yeast generates
699 an iron deprivation signal that is moderated by induction of the peroxiredoxin *TSA2*. J
700 Biol Chem. 2013;288: 11366–11377. doi:10.1074/jbc.M112.419259
701 54. Milgrom E, Diab H, Middleton F, Kane PM. Loss of vacuolar proton-translocating

ATPase activity in yeast results in chronic oxidative stress. J Biol Chem. 2007;282: 7125–7136. doi:10.1074/jbc.M608293200

55. Veatch JR, McMurray MA, Nelson ZW, Gottschling DE. Mitochondrial dysfunction leads to nuclear genome instability via an iron-sulphur cluster defect. Cell. 2009;137: 1247–1258. doi:10.1016/j.cell.2009.04.014

56. Valko M, Jomova K, Rhodes CJ, Kuča K, Musílek K. Redox- and non-redox-metal-induced formation of free radicals and their role in human disease. Arch Toxicol. 2016;90: 1–37. doi:10.1007/s00204-015-1579-5

57. Culotta VC, Howard WR, Liu XF. *CRS5* encodes a metallothionein-like protein in *Saccharomyces cerevisiae*. J Biol Chem. 1994;269: 25295–25302.

58. Pagani A, Villarreal L, Capdevila M, Atrian S. The *Saccharomyces cerevisiae* Crs5 Metallothionein metal-binding abilities and its role in the response to zinc overload. Mol Microbiol. 2007;63: 256–269. doi:10.1111/j.1365-2958.2006.05510.x

59. Chiaverini N, De Ley M. Protective effect of metallothionein on oxidative stress-induced DNA damage. Free Radic Res. 2010;44: 605–613. doi:10.3109/10715761003692511

60. Cai L, Koropatnick J, Cherian MG. Metallothionein protects DNA from copper-induced but not iron-induced cleavage in vitro. Chem Biol Interact. 1995;96: 143–155. doi:10.1016/0009-2797(94)03585-V

61. Tio L, Pagani MA, Atrian S. *Drosophila* proteins interacting with metallothioneins: a metal-dependent recognition. Proteomics. 2009;9: 2568–2577. doi:10.1002/pmic.200800729

62. Iraqui I, Kienda G, Soeur J, Faye G, Baldacci G, Kolodner RD, et al. Peroxiredoxin Tsa1 is the key peroxidase suppressing genome instability and protecting against cell death in *Saccharomyces cerevisiae*. PLoS Genet. 2009;5: e1000524.

727 doi:10.1371/journal.pgen.1000524

728 63. Game JC, Mortimer RK. A genetic study of X-ray sensitive mutants in yeast. Mutat Res.
729 1974;24: 281–292. doi:10.1016/0027-5107(74)90176-6

730 64. Mathiasen DP, Gallina I, Germann SM, Hamou W, Eléouët M, Thodberg S, et al.
731 Physical mapping and cloning of *RAD56*. Gene. 2013;519: 182–186.
732 doi:10.1016/j.gene.2013.01.044

733 65. Ametzazurra A, Larrea E, Civeira MP, Prieto J, Aldabe R. Implication of human N-α-
734 acetyltransferase 5 in cellular proliferation and carcinogenesis. Oncogene. 2008;27:
735 7296–7306. doi:10.1038/onc.2008.332

736 66. Neri L, Lasa M, Elosegui-Artola A, D'Avola D, Carte B, Gazquez C, et al. NatB-
737 mediated protein N-α-terminal acetylation is a potential therapeutic target in
738 hepatocellular carcinoma. Oncotarget. 2017;8: 40967–40981.
739 doi:10.18632/oncotarget.17332

740 67. Aksnes H, Drazic A, Marie M, Arnesen T. First things first: vital protein marks by N-
741 terminal acetyltransferases. Trends Biochem Sci. 2016;41: 746–760.
742 doi:10.1016/j.tibs.2016.07.005

743 68. Polevoda B, Norbeck J, Takakura H, Blomberg A, Sherman F. Identification and
744 specificities of N-terminal acetyltransferases from *Saccharomyces cerevisiae*. EMBO J.
745 1999;18: 6155–6168. doi:10.1093/emboj/18.21.6155

746 69. Helbig AO, Rosati S, Pijnappel PWWM, van Breukelen B, Timmers MHTH,
747 Mohammed S, et al. Perturbation of the yeast N-acetyltransferase NatB induces
748 elevation of protein phosphorylation levels. BMC Genomics. 2010;11: 685.
749 doi:10.1186/1471-2164-11-685

750 70. Van Damme P, Lasa M, Polevoda B, Gazquez C, Elosegui-Artola A, Kim DS, et al. N-
751 terminal acetylome analyses and functional insights of the N-terminal acetyltransferase

NatB. Proc Natl Acad Sci U S A. 2012;109: 12449–12454. doi:10.1073/pnas.1210303109

71. Caesar R, Warringer J, Blomberg A. Physiological importance and identification of novel targets for the N-terminal acetyltransferase NatB. Eukaryot Cell. 2006;5: 368–378. doi:10.1128/EC.5.2.368-378.2006

72. Mesecke N, Spang A, Deponte M, Herrmann JM. A novel group of glutaredoxins in the cis-Golgi critical for oxidative stress resistance. Mol Biol Cell. 2008;19: 2673–2680. doi:10.1091/mbc.E07

73. Izquierdo A, Casas C, Mühlenhoff U, Lillig CH, Herrero E. *Saccharomyces cerevisiae* Grx6 and Grx7 are monothiol glutaredoxins associated with the early secretory pathway. Eukaryot Cell. 2008;7: 1415–1426. doi:10.1128/EC.00133-08

74. Farber-Katz SE, Dippold HC, Buschman MD, Peterman MC, Xing M, Noakes CJ, et al. DNA damage triggers Golgi dispersal via DNA-PK and GOLPH3. Cell. 2014;156: 413–427. doi:10.1016/j.cell.2013.12.023

75. Rodrigues J, Banks P, Lydall D. Vps74 connects the Golgi apparatus and telomeres in *Saccharomyces cerevisiae*. G3 (Bethesda). 2018;8: 1807–1816. doi:10.1534/g3.118.200172

76. Aguilera A, García-Muse T. R loops: from transcription byproducts to threats to genome stability. Mol Cell. 2012;46: 115–124. doi:10.1016/j.molcel.2012.04.009

77. Wahba L, Amon JD, Koshland D, Vuica-Ross M. RNase H and multiple RNA biogenesis factors cooperate to prevent RNA:DNA hybrids from generating genome instability. Mol Cell. 2011;44: 978–988. doi:10.1016/j.molcel.2011.10.017

78. Boiteux S, Jinks-Robertson S. DNA repair mechanisms and the bypass of DNA damage in *Saccharomyces cerevisiae*. Genetics. 2013;193: 1025–1064. doi:10.1534/genetics.112.145219

777 79. Fujiki Y, Yagita Y, Matsuzaki T. Peroxisome biogenesis disorders: molecular basis for
778 impaired peroxisomal membrane assembly. Biochim Biophys Acta. 2012;1822: 1337–
779 1342. doi:10.1016/j.bbadis.2012.06.004
780 80. Bonekamp NA, Völkl A, Fahimi HD, Schrader M. Reactive oxygen species and
781 peroxisomes: struggling for balance. BioFactors. 2009;35: 346–355.
782 doi:10.1002/biof.48
783 81. Bülow MH, Wingen C, Senyilmaz D, Gosejacob D, Sociale M, Bauer R, et al.
784 Unbalanced lipolysis results in lipotoxicity and mitochondrial damage in peroxisome-
785 deficient *Pex19* mutants. Mol Biol Cell. 2018;29: 396–407. doi:10.1091/mbc.E17-08-
786 0535
787 82. Rahim RS, Chen M, Nourse CC, Meedeniya ACB, Crane DI. Mitochondrial changes
788 and oxidative stress in a mouse model of Zellweger syndrome neuropathogenesis.
789 Neuroscience. 2016;334: 201–213. doi:10.1016/j.neuroscience.2016.08.001
790 83. Huang M-E, Kolodner RD. A biological network in *Saccharomyces cerevisiae* prevents
791 the deleterious effects of endogenous oxidative DNA damage. Mol Cell. 2005;17: 709–
792 720. doi:10.1016/j.molcel.2005.02.008
793 84. Ragu S, Faye G, Iraqui I, Masurel-Heneman A, Kolodner RD, Huang M-E. Oxygen
794 metabolism and reactive oxygen species cause chromosomal rearrangements and cell
795 death. Proc Natl Acad Sci U S A. 2007;104: 9747–9752. doi:10.1073/pnas.0703192104
796 85. Erjavec N, Nyström T. Sir2p-dependent protein segregation gives rise to a superior
797 reactive oxygen species management in the progeny of *Saccharomyces cerevisiae*. Proc
798 Natl Acad Sci U S A. 2007;104: 10877–10881. doi:10.1073/pnas.0701634104
799 86. Lam YT, Aung-Htut MT, Lim YL, Yang H, Dawes IW. Changes in reactive oxygen
800 species begin early during replicative aging of *Saccharomyces cerevisiae* cells. Free
801 Radic Biol Med. 2011;50: 963–970. doi:10.1016/j.freeradbiomed.2011.01.013

802 87. McFaline-Figueroa JR, Vevea J, Swayne TC, Zhou C, Liu C, Leung G, et al.
803 Mitochondrial quality control during inheritance is associated with lifespan and mother-
804 daughter age asymmetry in budding yeast. Aging Cell. 2011;10: 885–895.
805 doi:10.1111/j.1474-9726.2011.00731.x
806 88. Molin M, Yang J, Hanzén S, Toledano MB, Labarre J, Nyström T. Life span extension
807 and H_2O_2 resistance elicited by caloric restriction require the peroxiredoxin Tsa1 in
808 *Saccharomyces cerevisiae*. Mol Cell. 2011;43: 823–833.
809 doi:10.1016/j.molcel.2011.07.027
810 89. Lauer C, Völkl A, Riedl S, Fahimi HD, Beier K. Impairment of peroxisomal biogenesis
811 in human colon carcinoma. Carcinogenesis. 1999;20: 985–989.
812 doi:10.1093/carcin/20.6.985
813 90. Frederiks WM, Vreeling-Sindelárová H, Van Noorden CJF. Loss of peroxisomes causes
814 oxygen insensitivity of the histochemical assay of glucose-6-phosphate dehydrogenase
815 activity to detect cancer cells. J Histochem Cytochem. 2007;55: 175–181.
816 doi:10.1369/jhc.6A7068.2006
817 91. Frederiks WM, Bosch KS, Hoeben KA, van Marle J, Langbein S. Renal cell carcinoma
818 and oxidative stress: the lack of peroxisomes. Acta Histochem. 2010;112: 364–371.
819 doi:10.1016/j.acthis.2009.03.003
820 92. Deori NM, Kale A, Maurya PK, Nagotu S. Peroxisomes: role in cellular ageing and age
821 related disorders. Biogerontology. 2018;19: 303–324. doi:10.1007/s10522-018-9761-9
822 93. Treco DA, Lundblad V. Preparation of yeast media. Curr Protoc Mol Biol. 2001;Chapter
823 13: Unit13.1. doi:10.1002/0471142727.mb1301s23
824 94. Sherman F. Getting started with yeast. Methods Enzymol. 2002;350: 3–41.
825 doi:http://dx.doi.org/10.1016/S0076-6879(02)50954-X
826 95. Brachmann CB, Davies A, Cost GJ, Caputo E, Li J, Hieter P, et al. Designer deletion

827 strains derived from *Saccharomyces cerevisiae* S288C: a useful set of strains and
828 plasmids for PCR-mediated gene disruption and other applications. Yeast. 1998;14:
829 115–132. doi:10.1002/(SICI)1097-0061(19980130)14:2<115::AID-
830 YEA204>3.0.CO;2-2
831 96. Henderson KA, Hughes AL, Gottschling DE. Mother-daughter asymmetry of pH
832 underlies aging and rejuvenation in yeast. Elife. 2014;3: e03504.
833 doi:10.7554/eLife.03504
834 97. Tong AHY, Boone C. High-throughput strain construction and systematic synthetic
835 lethal screening in *Saccharomyces cerevisiae*. Methods Microbiol. 2007;36: 369–386,
836 706–707. doi:10.1016/S0580-9517(06)36016-3
837 98. Schneider CA, Rasband WS, Eliceiri KW. NIH Image to ImageJ : 25 years of image
838 analysis. Nat Methods. 2012;9: 671–675. doi:10.1038/nmeth.2089
839 99. Dittmar JC, Reid RJD, Rothstein R. ScreenMill: a freely available software suite for
840 growth measurement, analysis and visualization of high-throughput screen data. BMC
841 Bioinformatics. 2010;11: 353. doi:10.1186/1471-2105-11-353
842 100. Mcmahon KW, Manukyan A, Dungrawala H, Montgomery M, Nordstrom B, Wright J,
843 et al. FASTA barcodes : a simple method for the identification of yeast ORF deletions.
844 Yeast. 2011;28: 661–671. doi:10.1002/yea.1894
845 101. Lea DE, Coulson CA. The distribution of the numbers of mutants in bacterial
846 populations. J Genet. 1949;49: 264–285.
847 102. Hall BM, Ma C, Liang P, Singh KK. Fluctuation AnaLysis CalculatOR (FALCOR): a
848 web tool for the determination of mutation rate using Luria-Delbrück fluctuation
849 analysis. Bioinformatics. 2009;25: 1564–1565. doi:10.1093/bioinformatics/btp253
850 103. Janssens GE, Meinema AC, González J, Wolters JC, Schmidt A, Guryev V, et al. Protein
851 biogenesis machinery is a driver of replicative aging in yeast. Elife. 2015;4: e08527.

852 doi:10.7554/eLife.08527

853 104. Huang DW, Sherman BT, Lempicki RA. Systematic and integrative analysis of large
854 gene lists using DAVID bioinformatics resources. Nat Protoc. 2009;4: 44–57.
855 doi:10.1038/nprot.2008.211

856 105. Huang DW, Sherman BT, Lempicki RA. Bioinformatics enrichment tools: paths toward
857 the comprehensive functional analysis of large gene lists. Nucleic Acids Res. 2009;37:
858 1–13. doi:10.1093/nar/gkn923

859 106. Supek F, Bošnjak M, Škunca N, Šmuc T. REVIGO summarizes and visualizes long lists
860 of Gene Ontology terms. PLoS One. 2011;6: e21800.
861 doi:10.1371/journal.pone.0021800

862 107. Usaj M, Tan Y, Wang W, VanderSluis B, Zou A, Myers CL, et al. TheCellMap.org: a
863 web-accessible database for visualizing and mining the global yeast genetic interaction
864 network. G3 (Bethesda). 2017;7: 1539–1549. doi:10.1534/g3.117.040220

865 108. Baryshnikova A. Systematic functional annotation and visualization of biological
866 networks. Cell Syst. 2016;2: 412–421. doi:10.1016/j.cels.2016.04.014

Figure captions

Fig 1. Combining the Mother Enrichment Program with high-throughput replica-pinning to screen for genes that suppress spontaneous mutations during yeast replicative aging. (A) The Mother Enrichment Program (MEP). Estradiol induction causes irreversible arrest of daughter cell proliferation, while growth of mother cells is unaffected. Inactivation of the MEP due to spontaneous mutations results in estradiol-insensitive cells called escapers. (B) Escaper formation is a readout for spontaneous mutation events during replicative aging. High-density arrays of MEP colonies are pinned on estradiol and escapers are subsequently detected by re-pinning on estradiol (big colonies). (C) Schematic of the screening procedure. The MEP is introduced into the YKO collection via Synthetic Genetic Array (SGA) methodology. The resulting MEP-YKO collection is amplified by high-throughput (HT) replica-pinning on estradiol, which activates the MEP and triggers replicative aging. A second replica-pinning on estradiol allows detection of escapers (escaper test). Escaper frequencies are calculated for each strain of the MEP-YKO collection. (D) Comparison of escaper frequencies of the whole MEP-YKO collection with escaper frequencies of wt and mutator (*msh3*) controls. (E) CLIK analysis sets an unbiased cutoff for validation. Green and blue colors indicate regions of the plot significantly enriched for physical and genetic interactions, while regions deprived of significant enrichment are plotted in gray. The red dotted line marks the cutoff suggested by the CLIK algorithm.

Fig 2. Overview of the general mutation suppression genes. (A) Functional enrichment in the yeast genetic landscape. Dotted lines indicate functional domains within the yeast genetic landscape, i.e. gene clusters enriched for a specific set of GO terms (the name of each functional domain is indicated by a colored label). Regions of the global similarity network significantly

891 enriched for genes exhibiting genetic interactions with general mutation suppression genes
892 were mapped using SAFE and are indicated in blue. (B) Gene Ontology enrichment analysis.
893
894 **Fig 3. Overview of the MEP-specific mutation suppression genes.** (A) Functional
895 enrichment in the yeast genetic landscape. Regions of the global similarity network
896 significantly enriched for genes exhibiting genetic interactions with MEP-specific mutation
897 suppression genes were mapped using SAFE and are indicated in orange. See Legend to Fig
898 2A for details. (B) Gene Ontology enrichment analysis.
899
900 **Fig 4. *PEX19* suppresses age-dependent accumulation of mutations.** (A) *CAN1* forward
901 mutation rate in young wt and *pex19*Δ cells. Values from three independent experiments are
902 plotted. The thick dark bars represent the median values. ns: non-significant. (B) Age-
903 dependent mutation frequencies at the *CAN1* locus in wt (replicative age ~17) and *pex19*Δ
904 (replicative age ~15.5) cells. The difference between observed and expected mutation
905 frequencies from four independent experiments is plotted. The horizontal bars represent the
906 median values. p-value was determined by Student's *t*-test.

Supporting information

S1 Fig. Exclusion of strains that escaped before the beginning of the screen. When serial dilutions of strains from the MEP-YKO collection are spotted in the presence of estradiol, growth of MEP-proficient strains is restricted, while escaper strains grow normally. An example of one MEP-proficient strain and one escaper is shown.

S2 Fig. Raw data for all the age-dependent mutation frequency measurement experiments. (A) Mutation frequencies at the *CAN1* locus in young and old cells from the indicated strains. In the case of old cells, both observed and expected mutation frequencies are shown. For each individual experiment, the median replicative age of the young and old cell populations is indicated. (B) Bud scars distribution of young and old cell populations from each experiment.

S3 Fig. *ICE2*, *ATG23* and *ROX3* did not validate as age-specific mutation suppression genes. (A) *CAN1* forward mutation rate in young wt, *ice2*Δ, *atg23*Δ, and *rox3*Δ cells. Mean values from three independent experiments are plotted. Error bars represent standard error. ns: non-significant. (B) Age-dependent mutation frequencies at the *CAN1* locus in wt (replicative age ~17), *ice2*Δ (replicative age ~15), *atg23*Δ (replicative age ~15.5), and *rox3*Δ (replicative age ~15) cells. The difference between observed and expected mutation frequency is plotted. For the wt, the mean value from four independent experiments is plotted. Error bars represent standard error. For the mutants, only one experiment is shown (see the Results and Material and Methods sections for details).

S4 Fig. *PEX3* deletion results in elevated spontaneous mutations in aged cells. (A) *CAN1* forward mutation rate in young wt, and *pex3*Δ cells. Mean values from three or four

independent experiments are plotted. Error bars represent standard error. ns: non-significant. (B) Age-dependent mutation frequencies at the *CAN1* locus in wt (replicative age ~17), and *pex3*Δ (replicative age ~13) cells. The difference between observed and expected mutation frequency is plotted. For the wt, the mean value from four independent experiments is plotted. Error bars represent standard error. For *pex3*Δ, only one experiment is shown.

S1 Table. ScreenTroll phenotypic enrichment analysis. ScreenTroll analysis (http://www.rothsteinlab.com/tools/screenTroll) identifies overlaps between published screens and our gene dataset (cutoff 75% escaper frequency, determined by CLIK). The top overlaps are related to genome instability and DNA damage sensitivity. "ORFs in screen" refers to the total number of hits identified in the overlapping screen.

S2 Table. List of putative age-specific mutation suppression genes.

S3 Table. Escaper formation is not always caused by mutations at the *cre-EBD78* locus.

S1 File. Complete escaper frequency data from the screen and validation of mutation suppression genes.

S2 File. SAFE enrichments and GO enrichment analysis for general and MEP-specific mutation suppression genes.

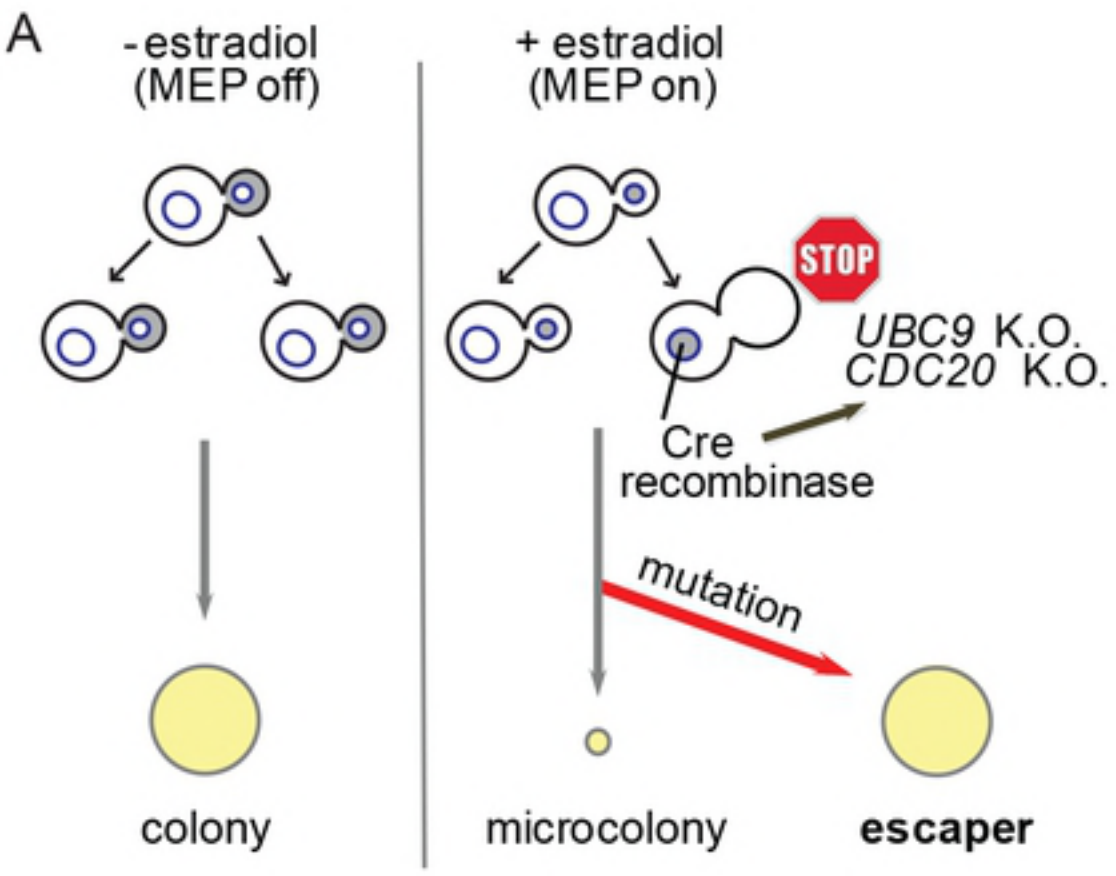

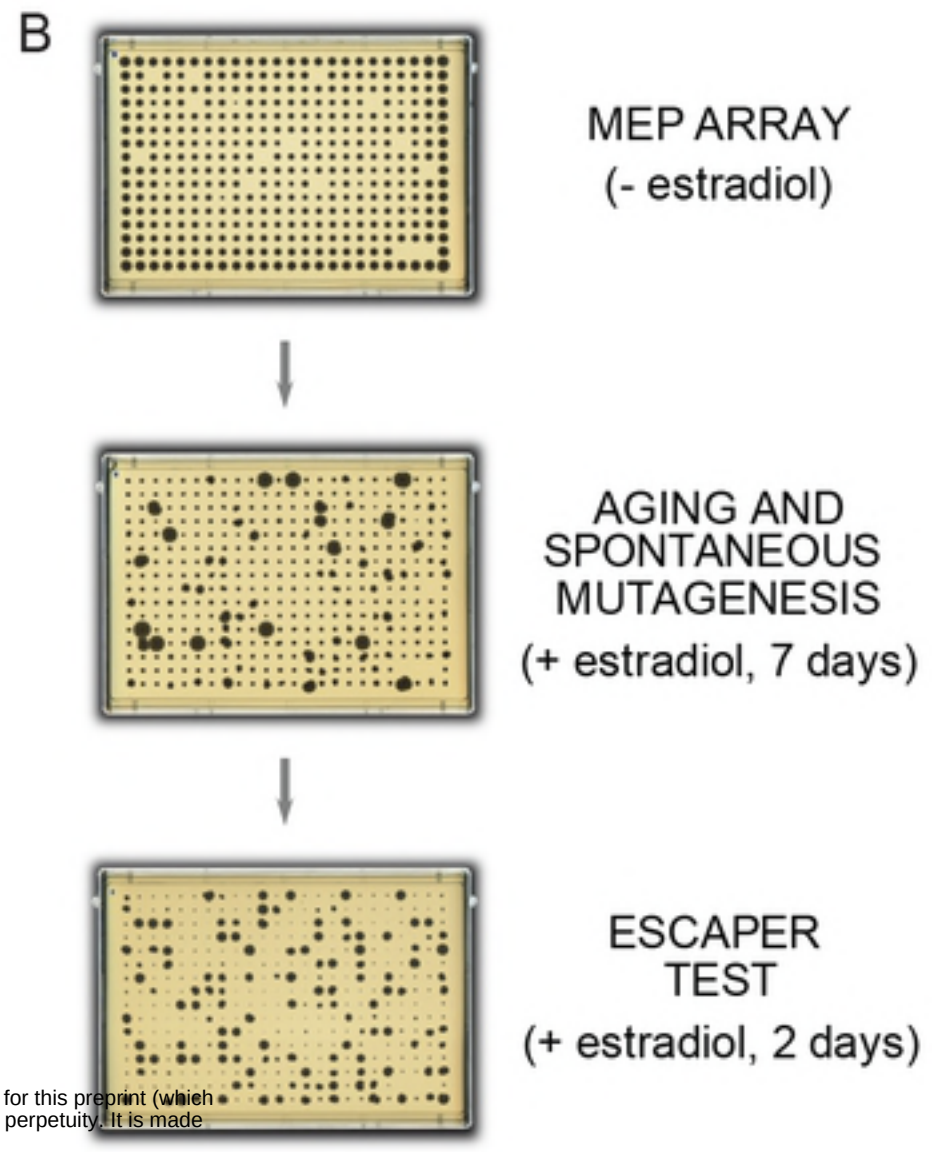

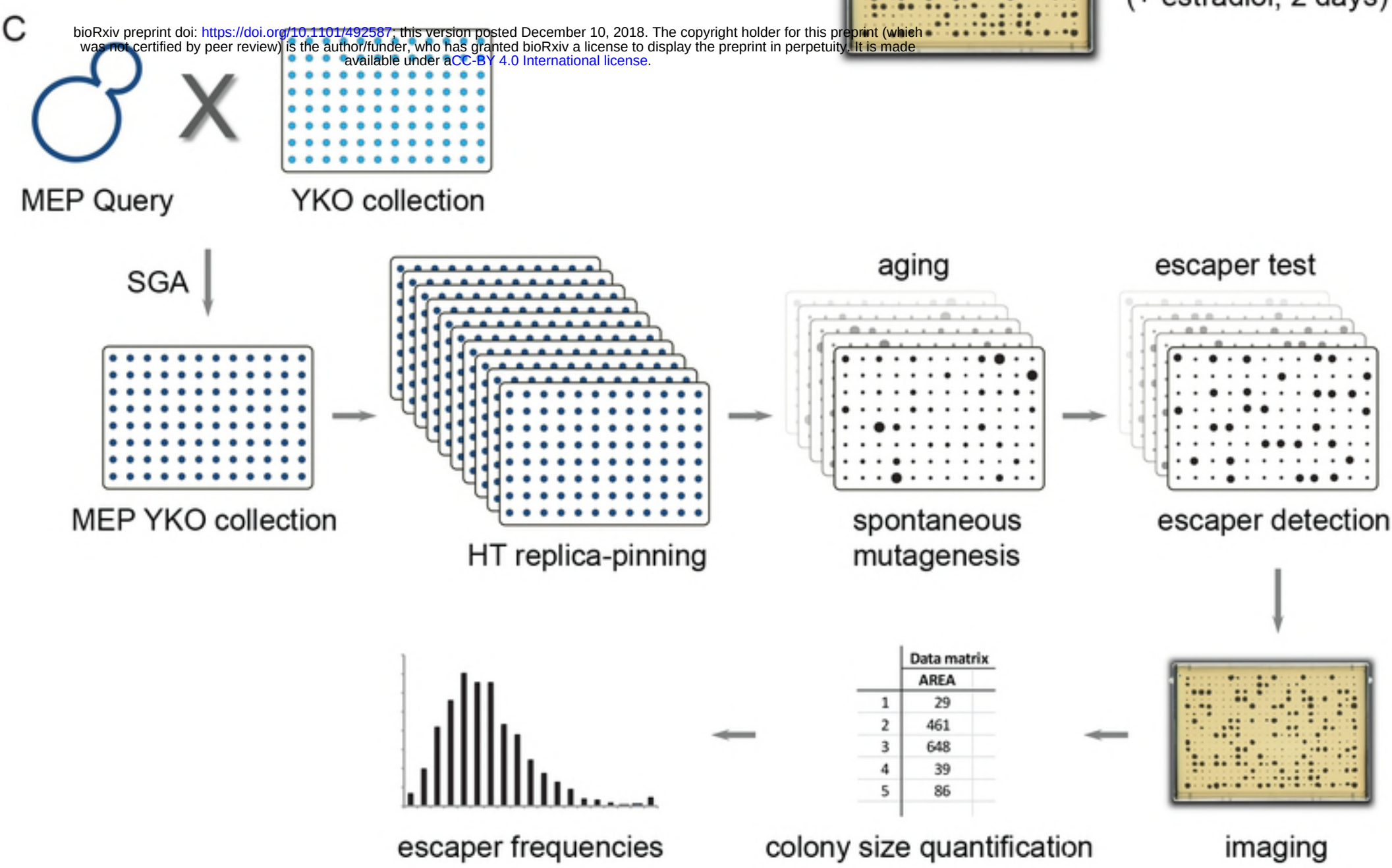

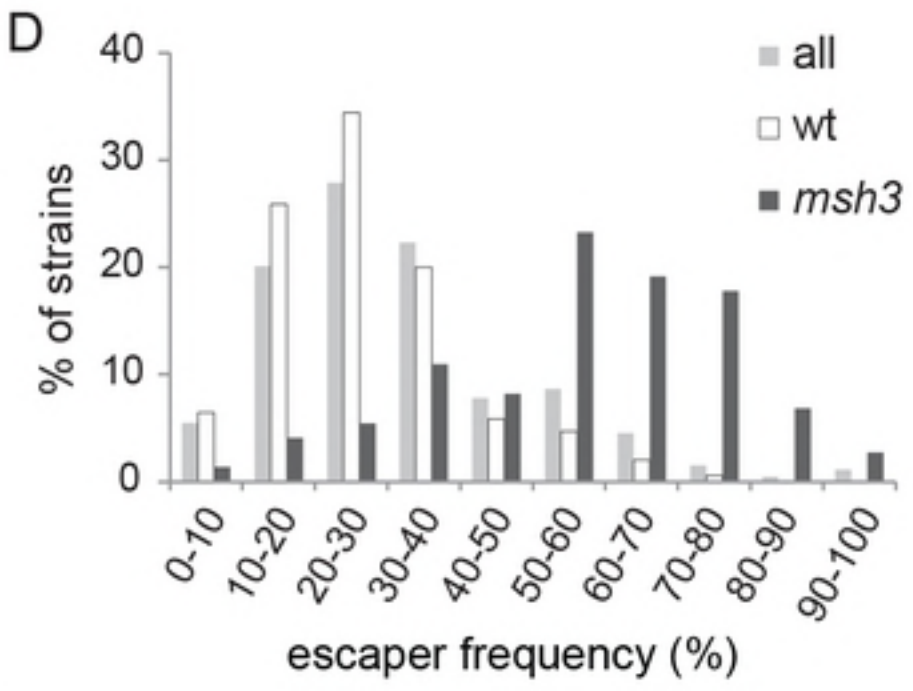

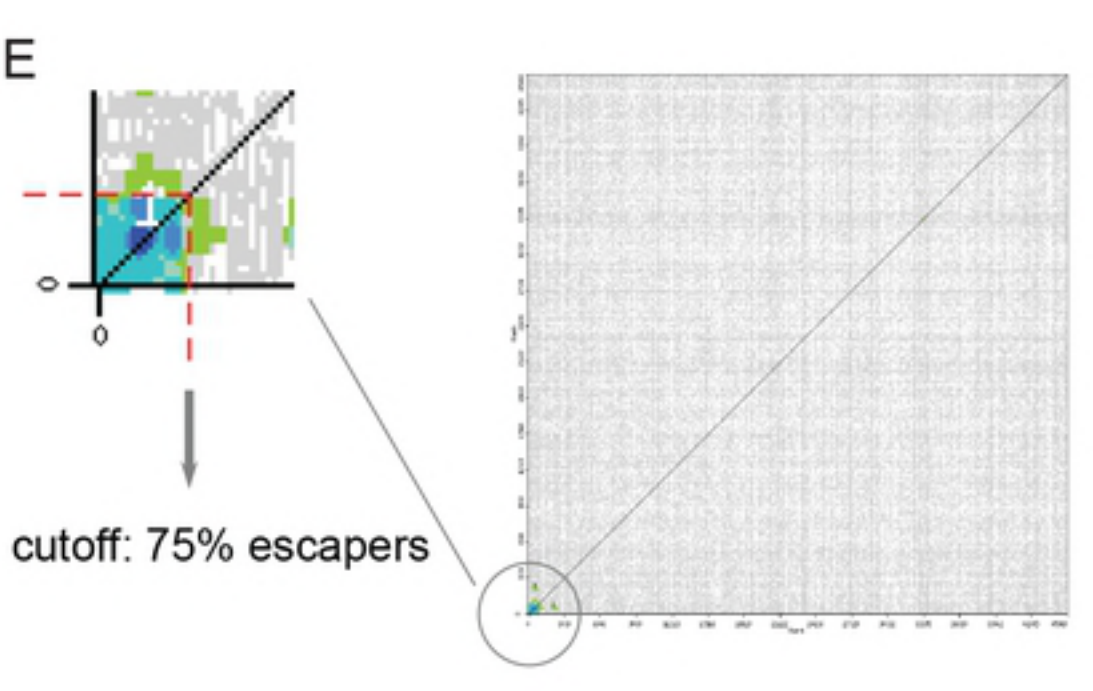

Figure 1

A

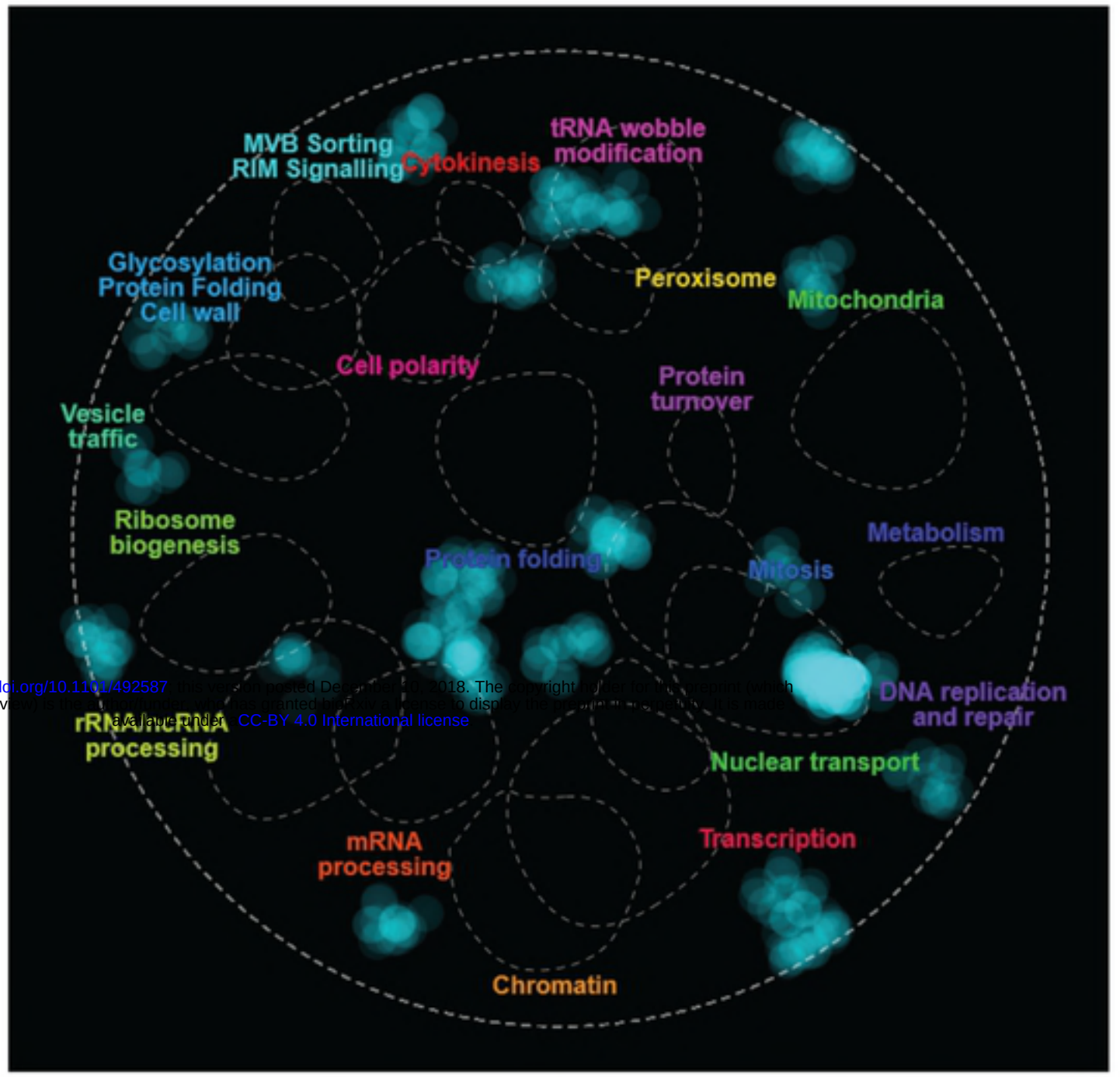

B

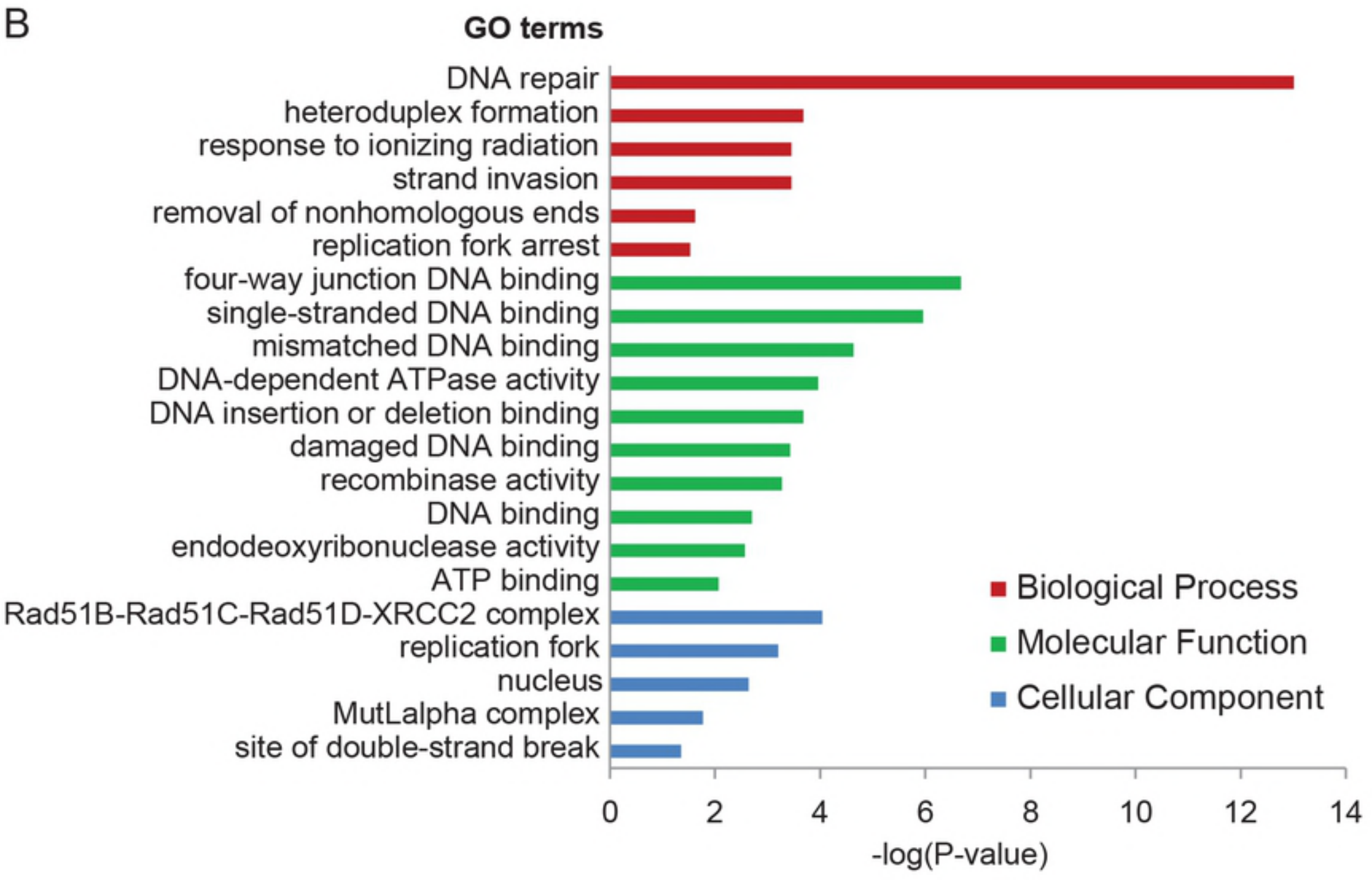

Figure 2

A

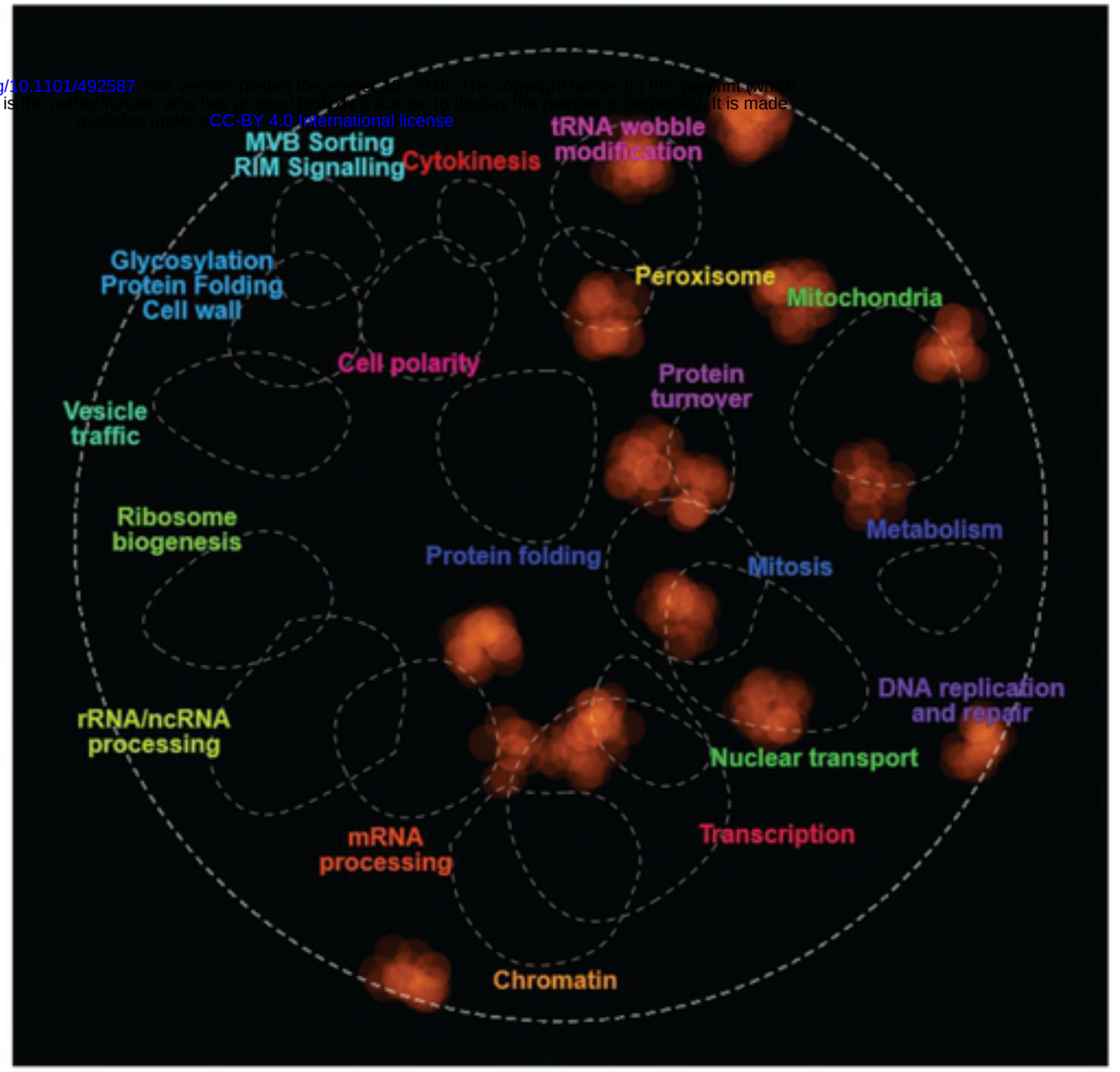

B

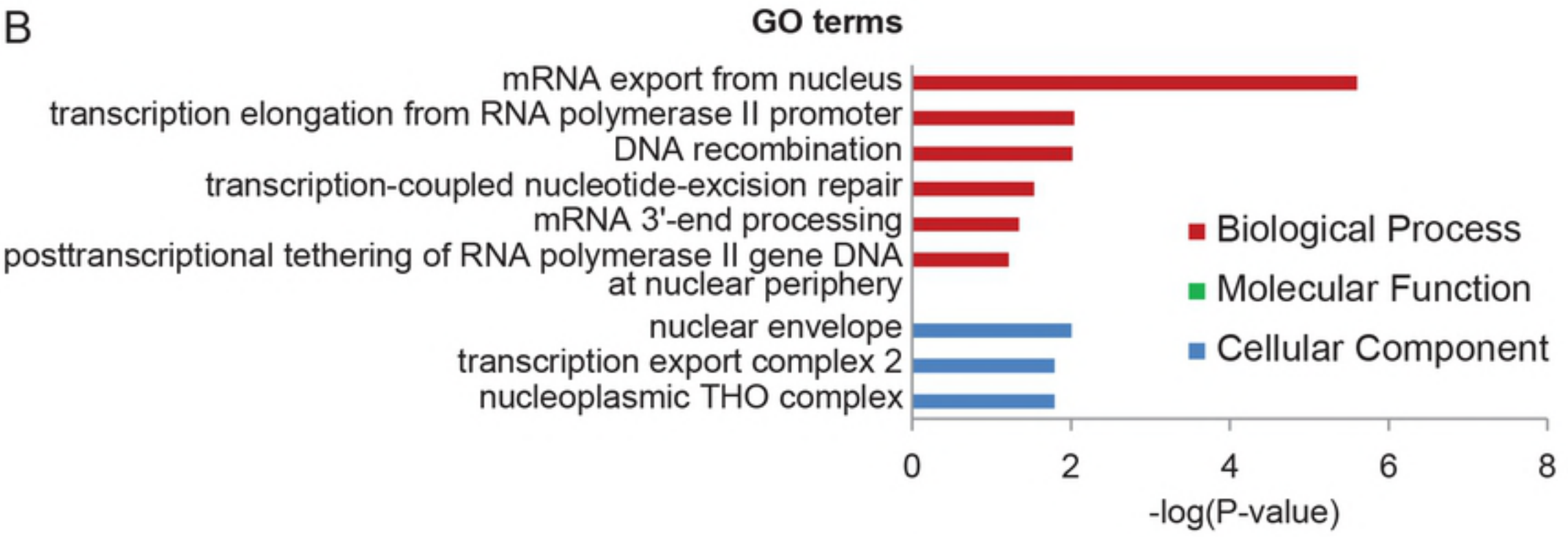

Figure 3

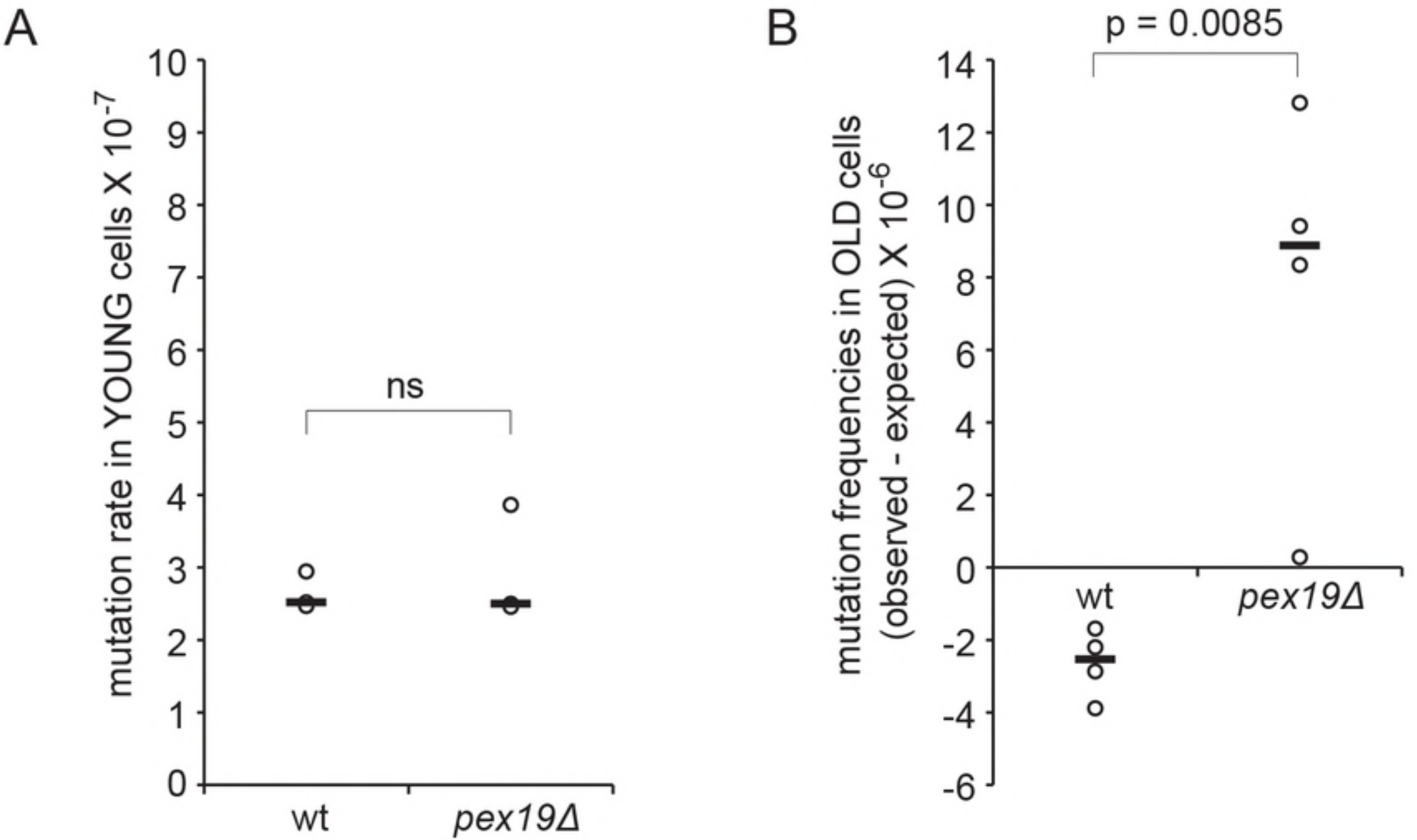
A
mutation rate in YOUNG cells X 10-7
10
9
8
7
6
5
4
3
2
1
0
ns
wt
pex19Δ
B
p = 0.0085
mutation frequencies in OLD cells
(observed - expected) X 10-6
14
12
10
8
6
4
2
0
-2
-4
-6
wt
pex19Δ

Figure 4